Prospects for antiferromagnetic spintronic devices

Pedram Khalili Amiri^{1#}, Charudatta Phatak^{2,3}, Giovanni Finocchio⁴

¹ Department of Electrical and Computer Engineering, Northwestern University; Evanston, Illinois, USA.

² Materials Science Division, Argonne National Laboratory; Lemont, Illinois, USA.

³ Department of Materials Science and Engineering, Northwestern University; Evanston, Illinois, USA.

⁴ Department of Mathematical and Computer Sciences, Physical Sciences and Earth Sciences, University of

Messina; Messina, Italy.

Email: pedram@northwestern.edu

Abstract

This article examines recent advances in the field of antiferromagnetic spintronics from the

perspective of potential device realization and applications. We discuss advances in the

electrical control of antiferromagnetic order by current-induced spin-orbit torques, particularly

in antiferromagnetic thin films interfaced with heavy metals. We also review possible scenarios

for using voltage-controlled magnetic anisotropy as a more efficient mechanism to control

antiferromagnetic order in thin films with perpendicular magnetic anisotropy. Next, we discuss

the problem of electrical detection (i.e., readout) of antiferromagnetic order, and highlight

recent experimental advances in realizing anomalous Hall and tunneling magnetoresistance

effects in thin films and tunnel junctions, respectively, which are based on noncollinear

antiferromagnets. Understanding the domain structure and dynamics of antiferromagnetic

materials is essential for engineering their properties for applications. For this reason, we then

provide an overview of imaging techniques as well as micromagnetic simulation approaches

for antiferromagnets. Finally, we present a perspective on potential applications of

antiferromagnets for magnetic memory devices, terahertz sources, and detectors.

1

I. Introduction

Spintronics broadly encompasses materials, heterostructures, and devices where spin and electronic (i.e., charge) transport are intricately coupled ¹. Over the past few decades, the field of spintronics has been largely the domain of ferromagnetically ordered materials. The reason is the typically large room-temperature macroscopic magnetization of ferromagnets such as Ni, Co, Fe, and their alloys, which emerges from the collective ordering of individual electron spins due to exchange interaction. This magnetization, besides being readily measurable in thin films and heterostructures using an array of magnetometry and microscopy techniques, also provides a useful experimental knob to control the underlying spintronic phenomena using an external magnetic field.

Several discoveries initiated and grew the thriving research field of ferromagnetic (FM) spintronics. Among these, the discoveries of giant magnetoresistance (GMR) ^{2, 3}, followed by the theoretical prediction ⁴ and experimental realization of giant room-temperature tunneling magnetoresistance (TMR) ^{5,6} played key roles, as they provided sizeable means to affect charge transport (i.e., electrical resistance) by magnetization, and thereby by an external magnetic field. These were followed by the discovery of a range of phenomena that allowed the inverse process, i.e., electrical control of the collective magnetization state using various types of torques, including spin-transfer torque (STT) 7,8, spin-orbit torque (SOT) 9,10, electric-field-induced (i.e., voltage-controlled) magnetization ¹¹ or magnetic anisotropy (VCMA) ¹²⁻¹⁴, piezoelectric and multiferroic effects ^{15, 16}, and other mechanisms. These phenomena collectively provided a way to both electrically detect (i.e., read) and manipulate (i.e., write) information into ferromagnetic devices. This combination of electrical detection and manipulation, in turn, enabled a wide range of applications which have been the subject of active research and development over the past three decades. Among these are magnetic field sensors based on spin valves, which made the tremendous growth of bit density in hard disk drives possible, paving the way for today's data centers and computing applications such as machine learning (ML) and artificial intelligence (AI). Another example is magnetic random-access memory (MRAM) which uses TMR for readout of information, and current- or voltage-controlled switching mechanisms for writing of information in nanoscale magnetic tunnel junctions

(MTJs) ^{17, 18}, and is being produced by major semiconductor manufacturers today. Other devices that are still mostly in the research or development stage include spintronic oscillators and spin diodes (detectors), where magnetoresistance, current-induced spin torques, or VCMA effects work in tandem to create interesting high-frequency properties with numerous potential applications ^{14, 19-23}.

By contrast, electrical manipulation and detection of antiferromagnetic (AF) order was thought to be necessarily inefficient, due to the vanishing macroscopic magnetization of antiferromagnetic materials. As a result, while many of the above-mentioned types of devices could benefit from using antiferromagnetic rather than ferromagnetic materials (e.g., faster and more scalable memory devices, and detectors or oscillators that operate at THz frequencies and room temperature), such devices were thought to be impractical until recently.

The use and impact of antiferromagnetic materials ²⁴ is being reexamined in the light of new discoveries, some of which we review in this article. These include experiments that demonstrated electrical control of antiferromagnetic order in a range of insulating and metallic antiferromagnetic materials ²⁵⁻³⁸, as well as recent theoretical and experimental work ³⁹⁻⁵⁴ that is opening new possibilities for reliable electrical readout of antiferromagnetic order. This review aims to provide an introduction to these developments from the perspective of using antiferromagnetic materials in useful devices, particular for memory and computing. It is therefore not meant to be a comprehensive accounting of all active research directions in antiferromagnetic spintronics, for which we refer the reader to other recent reviews.

The paper is organized as follows. Section II introduces the basic concepts of antiferromagnetic materials and some of their existing manipulation and readout mechanisms, which will be discussed in more detail in later sections. Sections III and IV then discuss recent advances in electrical control of magnetic order in antiferromagnets. Section V focuses on electrical readout, focusing on the case of noncollinear antiferromagnets, which are a subset of antiferromagnetic materials that have recently seen significant progress towards practical device applications. Sections VI and VII then present some of the microscopy and micromagnetic modeling tools that allow one to study antiferromagnetic materials. Finally, in Section VIII we present a perspective on the technological need and application perspectives

of antiferromagnetic spintronic devices, particularly for memory and THz device applications.

II. Antiferromagnets as the active element of spintronic devices

In general, an antiferromagnetic material has two or more sublattices, the magnetizations of which ideally add up to zero in the absence of any external fields, i.e., $\sum_{i=1}^{N} M_i = 0$, where N is the number of sublattices and M_i is the magnetization of the i-th sublattice. The simplest case is that of a collinear antiferromagnet with N=2, where the two sublattices are separated by 180° , pointing in opposite directions. The order parameter (or state variable, when used in an information processing device) in this case is the Néel vector $S=M_1-M_2$, which is often normalized by the sum of the magnetization values, M_1+M_2 . Note that collinear ferrimagnets are a subset of these where $M_1 \neq M_2$. This is illustrated in Fig. 1.

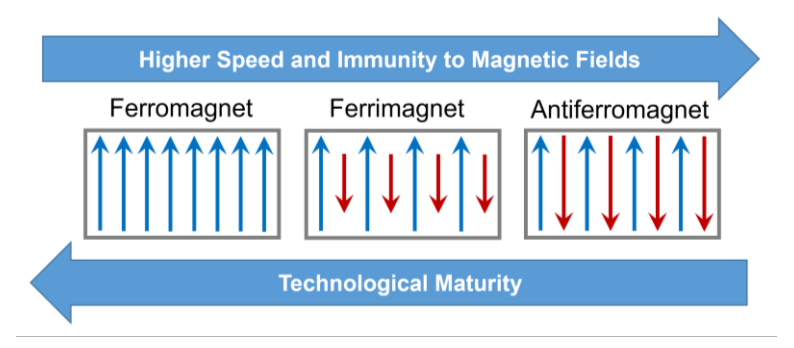


Fig. 1. Schematic illustration of three basic types of magnetic order in materials with one or two sub-lattices.

Many antiferromagnetic materials of interest, including some of those discussed in later sections, however, are noncollinear and have more than two sublattices. Two examples of the XMn₃ family of metallic antiferromagnets (where in this case, X is Ir or Sn) are shown in Fig. 2. In these materials, the definition of the Néel vector, i.e., state variable, can be generalized to $S=M_1+R_{2\pi/3}M_2+R_{4\pi/3}M_3$, where $R_{2\pi/3}$ and $R_{4\pi/3}$ represent rotation operators by 120° and 240° angles, respectively ⁵⁵⁻⁵⁷. This vector is also referred to as the octupole magnetic moment, and is particularly relevant to the properties of certain noncollinear materials in terms of electrical readout of antiferromagnetic order ^{39, 46, 48, 58}, as discussed in Section V.

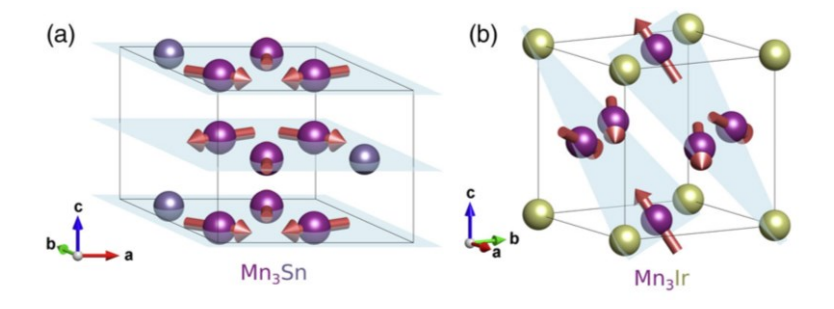


Fig. 2. Illustration of the noncollinear spin configuration in two antiferromagnets of the XMn₃ family discussed in this review. Reproduced with permission ⁴⁹.

III. Electrical manipulation of antiferromagnets by current-induced spin-orbit torque

Due to their vanishing net magnetization, antiferromagnetic materials do not interact efficiently with external magnetic fields, which can readily manipulate ferromagnetic order. The technological interest in antiferromagnetic spintronics grew when a number of experiments demonstrated that current-induced spin polarization can indeed interact with Néel order. While initial experiments focused on the so-called Néel SOT which originates in the bulk of certain antiferromagnetic materials ^{32, 33, 35-37, 59}, the focus of this review are structures where an antiferromagnetic layer is interfaced with a heavy metal (or other material with large spin-orbit interaction), where an interfacial SOT allows for manipulation of the Néel order in the presence of electric current ^{25-27, 58, 60}. The structure of these devices, shown schematically in Fig. 3, is reminiscent of ferromagnetic SOT-MRAM devices that have three electrical terminals, with separate read and write paths. This separation, while sacrificing bit density, is beneficial as it ensures a higher endurance of the readout path (typically, a tunnel junction), which does not experience the large write currents used to switch the antiferromagnetic layer ⁶¹.

A picture of an early experiment of this type is shown in Fig. 4a, where the antiferromagnetic and heavy metal layers are PtMn and Pt, respectively ²⁶. PtMn was chosen as the antiferromagnetic layer in this experiment due to its compatibility with established silicon manufacturing. Write currents are passed in opposite directions along one pair of pads (A and A', or B and B'). A smaller alternating (AC) read current is then applied along the other two terminals, which causes oscillations of the Néel vector at the same frequency as the current. Combined with the anisotropic magnetoresistance (AMR) of the PtMn film, the result is a

measurable AC voltage at twice the frequency of the input. This allows one to electrically read out the Néel vector orientation, as shown in Fig. 4b; however, the small readout margin provided by AMR and the need for an AC read current severely limited the potential of this structure as a practical memory device, as explained further below.

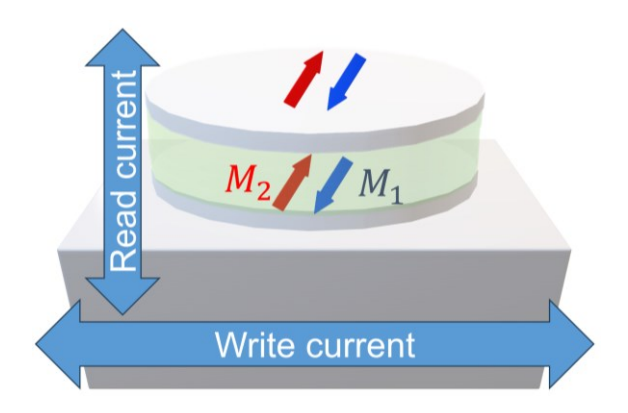


Fig. 3. Schematic illustration of a three-terminal antiferromagnetic tunnel junction with separate electrical read and write paths.

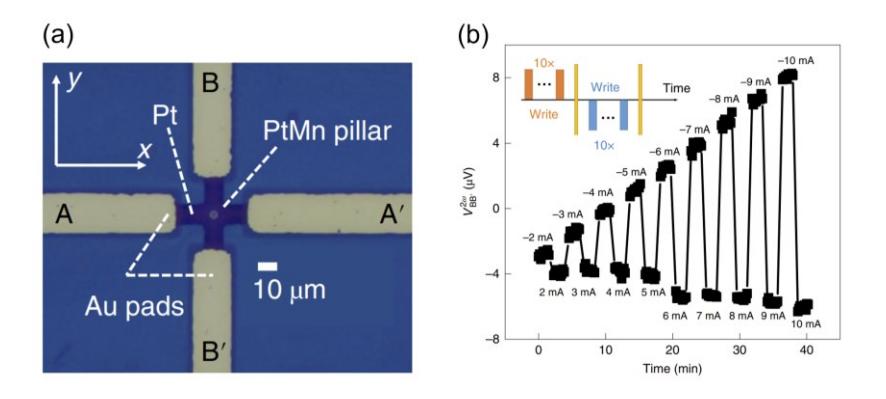


Fig. 4. (a) Device structure and (b) electrical current-induced switching results in antiferromagnetic PtMn pillars switched by electrical currents injected into an adjacent Pt layer. Reproduced with permission ²⁶.

The switching data shown in Fig. 4b indicate a gradual change of the antiferromagnetic order in response to electric current. This feature, which was a common characteristic of many early experiments on current-induced antiferromagnetic switching in relatively large devices, can be understood in terms of a domain-mediated switching mechanism where currents

manipulate the average Néel vector throughout the antiferromagnetic layer, but do not succeed in fully reorienting (i.e., saturating) it ^{25, 26, 28, 35}. A representative micromagnetic simulation of this domain-mediated switching mechanism in the case of Pt/PtMn pillars is shown in Fig. 5. The magnetoelastic energy due to the substrate and the easy plane magnetocrystalline anisotropy allow the stabilization of metastable states, which are characterized by complex domain wall patterns that involve vortices (V) and anti-vortices (AV).

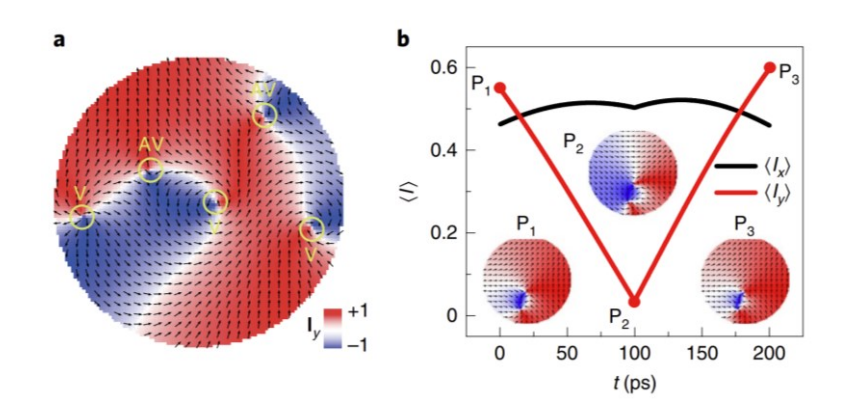


Fig. 5. Micromagnetic simulation results of (a) domain structure, including vortex (V) and antivortex (AV) textures, in a PtMn pillar, and (b) reversible modification of the domain pattern in response to a current-induced spin-orbit torque. Reproduced with permission ²⁶.

The current-induced manipulation of Néel order in the Pt/PtMn material system was also studied in devices with a slightly different geometry ²⁷, where in addition to electrical readout, the effect of current-induced SOT on the antiferromagnetic domains was directly observed using photoemission electron microscopy (PEEM) magnetic linear dichroism experiments, which further confirmed the above picture.

Overall, these results emphasized the need for better understanding of the micromagnetic domain structure of the Néel vector in antiferromagnetic materials, its dependence on film deposition and processing conditions, and its interaction with electrical signals. Such an understanding can be gained by direct imaging techniques aided by micromagnetic simulations, which will be the topics of Sections VI and VII, respectively.

The above experiments confirmed the encouraging possibility of electrical switching of

Néel vectors in silicon-compatible antiferromagnetic materials, which was an important step towards practical device concepts for memory and computing applications. At the same time, they clearly showed the difficulty of reliably reading out the Néel vector orientation by electrical signals, due to the small magnitude of the AMR effect. A second issue compounding this difficulty was the fact that very high current densities were required for switching the antiferromagnet in many experiments of this type, which in turn, can cause to non-magnetic artifacts in the measurement, e.g., due to electromigration and thermal effects within the device 25, 28, 62

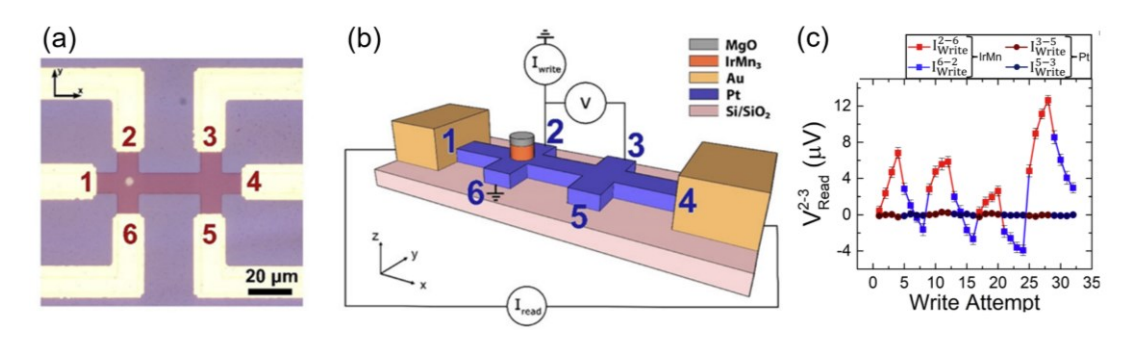


Fig. 6. (a) Device photograph, (b) schematic of the electrical test configuration, and (c) experimental current-induced switching results in a Pt/IrMn₃-based device structure. Switching is only observed when currents are applied to the cross which contains the antiferromagnetic pillar, confirming the magnetic origin of the observed switching signal. Reproduced with permission ²⁵.

To ensure that the observed switching was indeed magnetic in origin, a subsequent work proposed a six-terminal double-cross device structure, where the antiferromagnetic pillar is placed on only one of the two Pt crosses ²⁵, as shown in Figs. 6a and 6b. The additional terminals and the presence of a Pt-only cross within the device allow for performing an in-situ control experiment. In this case, write currents can be applied along terminals 2 and 6, in which case they will pass under the antiferromagnetic pillar on the left cross, or along terminals 3 and 5, in which case they will pass through the Pt-only cross without any interaction with the antiferromagnetic layer. Readout can be performed by applying a small read current along terminals 1 and 4, and reading the differential voltage between terminals 2 and 3. The results

of this differential readout approach in the case of the Pt/IrMn₃ materials combination are shown in Fig. 6c. A wide range of current densities was observed to result only in switching of the IrMn₃ pillar, without switching the adjacent Pt layer. Larger current densities were, however, indeed observed to switch also the Pt layer, as expected. Similar results were recently obtained in the case of a Pt/PtMn₃ materials combination ⁶³, illustrating that this approach can be generally applied to a wide range of antiferromagnetic materials with a pillar geometry deposited on a heavy metal. Note also that, in both of these six-terminal experiments, the selected antiferromagnetic material had a noncollinear spin configuration, as seen in Fig. 2.

It is worth emphasizing that all current-induced antiferromagnetic switching experiments discussed above were performed in the absence of magnetic bias fields. This is in sharp contrast to the case of ferromagnetic SOT-MRAM, where deterministically switching the magnetic free layer (which typically needs to be perpendicularly magnetized for long-term data retention) requires a symmetry-breaking in-plane magnetic bias field ^{61, 64, 65}. This bias field can be challenging to realize on a semiconductor chip, and is a source of device-to-device variations. The natural field-free operation of the antiferromagnetic SOT devices shown above is thus a highly beneficial feature.

IV. Electrical manipulation of antiferromagnets by electric fields

Current-induced manipulation of magnetic order, whether antiferromagnetic or ferromagnetic, presents certain challenges ^{66, 67}. The most important of these are the Ohmic energy dissipation due to the large write current, and the fact that underlying access transistors (which are required to isolate the selected bits) must large enough to drive this current. As a result, switching of magnetic order by electric fields is an appealing alternative, which could potentially solve both problems at once ^{12, 68-70}.

Much progress has been made in electric-field-induced switching of ferromagnetic memory devices using the voltage-controlled magnetic anisotropy (VCMA) effect in recent years. The VCMA effect relies on the electric-field-induced modulation of the interfacial perpendicular magnetic anisotropy (PMA) at the surface of metallic ferromagnets interfaced with an oxide ⁷¹. In the case of perpendicularly magnetized CoFeB free layers interfaced with

an MgO tunnel barrier, which is the most common material system used for MRAM today ⁷²⁻⁷⁴, the PMA typically shows an odd behavior on the applied electric field. As a result, one polarity of applied voltage increases the PMA and stabilizes the out-of-plane magnetized free layer, while the opposite polarity reduces the PMA, thereby facilitating switching.

VCMA at the CoFeB-MgO interface of two-terminal CoFeB/MgO/CoFeB magnetic tunnel junctions has been used to drive the magnetization into a precessional motion around an inplane applied magnetic field, which can result in 180° switching of the magnetization when the voltage pulse is timed to half the precession period of the free layer ^{12, 67}. The same effect can also be used to generate random numbers with a fast bit rate of ~10 ns/bit, provided the applied voltage is kept long enough to allow the magnetization to reorient to the in-plane direction ⁷⁵. True random numbers generated with the latter approach have been shown to pass the NIST Statistical Test Suite (STS) and have been utilized in recent demonstrations of physically unclonable functions ⁷⁶ and solving integer factorization problems using a probabilistic computing approach ⁷⁵.

In addition to switching or random number generation in single-domain ferromagnets, the modulation of PMA by electric fields due to VCMA also allows for control over magnetic textures and magnetization dynamics, the properties of which are sensitive to the PMA value in thin magnetic films. For example, VCMA has been used to stabilize and annihilate skyrmions using an applied voltage ^{78, 79}. Since propagating magnons (spin waves) in a magnetic material are topologically scattered by a skyrmion (with a scattering angle determined by the skyrmion topological charge) ^{80, 81}, the latter effect can also be utilized to realize a voltage-controlled skyrmionic magnonic switch, which can divert magnons within a magnetic network of wires ⁸². VCMA can also be used to modify the resonance frequency of ferromagnetic elements driven by a radio-frequency signal, and even as the main driving force driving the resonance ¹⁴, which has been shown to enable spintronic microwave detectors (spin diodes) with very high sensitivity ²⁰.

It is important to note, however, that the concept of VCMA is not unique to ferromagnets. Computational studies have indicated the possibility of large VCMA coefficients at interfaces of antiferromagnetic materials such as FeRh and PtMn ^{83, 84}. If successfully realized in a device

geometry, VCMA-induced or VCMA-assisted switching of antiferromagnets could alleviate many of the issues associated with high write current densities listed in Section III.

A proposed device concept is shown in Fig. 7 ⁸⁵. An antiferromagnetic free layer with PMA is interfaced with an insulator. When a voltage pulse is applied across the insulator, the two sublattices of the antiferromagnetic layer are driven into a coupled resonant motion. Importantly, while the threshold electric field for inducing these dynamics is determined by the PMA (which can be on the same order as that in ferromagnetic free layers), their frequency is determined by the exchange interaction between the sublattices, and can therefore be much higher than in the ferromagnetic case. This is a distinct advantage over both ferromagnetic VCMA devices where the resonance frequency is typically in the GHz range, and over antiferromagnetic SOT devices, where accessing the higher (sub-) THz dynamics requires very large current densities. Similar to the case of the ferromagnetic VCMA devices, a timed pulse that coincides with approximately half the precession period of these dynamics can switch the antiferromagnetic order to its opposite state, with write times on the order of tens of picoseconds, as opposed to ~1 ns which is typical for ferromagnetic VCMA-MRAM ⁸⁵.

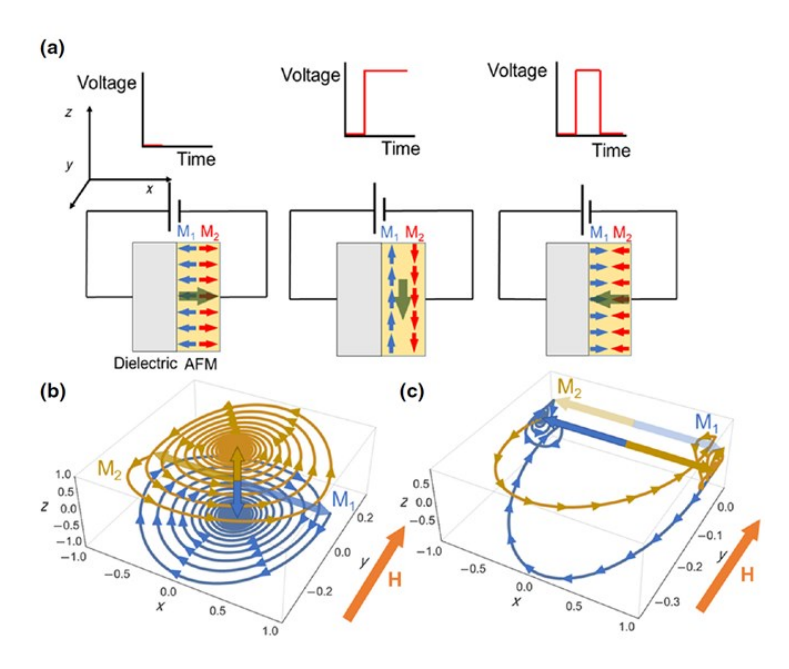


Fig. 7. (a) Concept and (b, c) simulation results illustrating a strategy for VCMA-induced switching of antiferromagnetic memory devices. The modification of interfacial anisotropy by electric field can reorient the Néel vector by 90° for long voltage pulses, while it can switch it

by 180° if the voltage pulse coincides with approximately half the precession period of the antiferromagnetic dynamics (in this case ~30 ps). Reproduced with permission ⁸⁵.

V. Electrical readout of magnetic order in noncollinear antiferromagnets

The general structure of a potential antiferromagnetic memory device is shown in Fig. 3. Whether writing of information (i.e., switching of the antiferromagnetic state) is achieved by using electric currents or voltages, efficient electrical readout is also a key requirement for a viable device concept. This is important not only for memory and computing devices, where having an electrical characteristic (e.g., resistance) that is sensitive to the direction of the Néel vector is required for reading the stored information ⁸⁶, but also for an array of ultrafast proposed antiferromagnetic devices that utilize either single-domain exchange-enhanced antiferromagnetic dynamics or antiferromagnetic textures (e.g., skyrmions) ⁸⁷⁻⁹⁰. Potential applications include the realization of (sub-) THz sources and detectors, going beyond the frequency range that is attainable with ferromagnets. Such devices can be potential candidates for filling the "THz gap" for communications and sensing applications, as discussed in Section VIII.

In the context of memory devices, having a sizeable electrical readout mechanism is essential. The latter is often defined as an on/off or magnetoresistance (MR) ratio $\Delta R/R$, which quantifies the difference between electrical resistance characteristics in the two states of the device (ΔR) – for example, corresponding to two Néel vector orientations – relative to its baseline value (R). The importance of this ratio derives from the fact that larger $\Delta R/R$ values can result in easier and faster readout by electrical circuits, for example by sensing a voltage difference of the two states when a readout current is applied to the device. In addition, a large $\Delta R/R$ value helps eliminate overlap between the statistical distributions of on and off (i.e., low and high resistance) states across large numbers of devices ⁹¹. As a result, the larger the number of devices on a chip (e.g., the memory capacity needed for an application), the larger the TMR ratio typically has to be for reliable memory operation.

The structure of Fig. 3 schematically illustrates a potential solution to this problem, namely, by building a structure which is analogous to the widely used ferromagnetic MTJs. Here, the

bottom antiferromagnetic layer has a Néel vector that can be electrically manipulated (e.g., by SOT as discussed in Section III), while its relative orientation with respect to a top (fixed) Néel vector is read resistively. Other possibilities for readout of the Néel vector in such a device might include anomalous Hall effect (AHE) or GMR, which are again analogous to their ferromagnetic counterparts. Naively, one might assume the TMR, GMR, or AHE in such an all-antiferromagnetic memory device concept to be nearly zero, due to the absence of macroscopic magnetization in antiferromagnetic materials. However, an increasing number of recent theoretical and experimental advances call this assumption into question.

Recent reports show that AHE can, in fact, be understood as a topological property of the material that follows from the Berry curvature of its band structure, and is therefore not limited to the normally considered ferromagnetic AHE effect ^{47, 50-52, 54, 58}. Several experiments have provided experimental evidence for this. For example, anomalous Hall readout of the antiferromagnetic state has been observed in Mn₃Sn, which is a noncollinear antiferromagnetic Weyl semimetal ⁵⁰. Switching in this case was performed by using the finite magnetic moment which arises from the tilting of the noncollinear moments, although it was argued that the large size of the observed AHE effect could not necessarily be explained by this small magnetization. Interestingly, this effect was also observed in the case of polycrystalline sputter-deposited Mn₃Sn films, where the magnetization could be controlled by current-induced spin-orbit torque ⁵⁸, similar to the experiments discussed in Section III. It is worth noting that the same noncollinear antiferromagnet was also shown to exhibit thermal ⁴⁸ and optical ⁴⁶ characteristics that are normally associated with macroscopic magnetization.

Measurement of the AHE effect, however, necessitates a multi-terminal device structure where the transverse voltage in response to a longitudinal reading current can be sensed electrically. This does not lend itself well to memory applications, where the number of leads to each device should be minimized to reduce the effective bit area. A more common approach followed in the case of ferromagnetic MRAM, therefore, has been to read out the free layer state by TMR, as shown in Fig. 3. In ferromagnets, TMR is understood in terms of the net spin polarization of the current, which is preserved through the tunneling process. Due to the asymmetry of the density of states of majority and minority spins on the receiving side, this

then results in different resistance levels depending on the relative magnetization directions of the two ferromagnets. In collinear antiferromagnets such as those shown in Fig. 1, such a spin polarization is not expected since the two sublattices have magnetizations that exactly cancel out. Recent theoretical works, however, have shown that a spin-polarized current analogous to that of ferromagnets is in fact possible in collinear antiferromagnets, provided certain symmetries are broken ^{53, 92, 93}. These types of materials, which have recently been termed "altermagnets", can therefore be expected, in principle, to also exhibit TMR in an appropriately engineered tunnel junction. The presence of a net spin current created by charge currents in altermagnetic RuO₂ has recently been shown experimentally, where an adjacent ferromagnetic layer was used to detect the spin polarization ⁴².

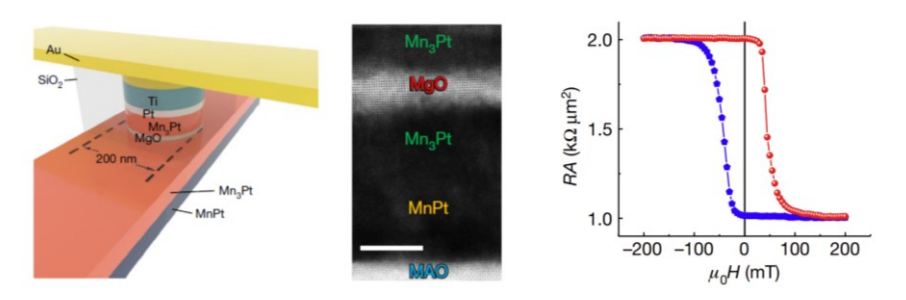


Fig. 8. Tunnel magnetoresistance in PtMn₃/MgO/PtMn₃ antiferromagnetic tunnel junctions epitaxially grown on a MgAl₂O₄ (MAO) substrate. Switching is performed by a ~0.1 T magnetic field, as shown in the right panel. Reproduced with permission ⁴⁰.

Another approach to realizing TMR in antiferromagnets has involved the use of noncollinear antiferromagnets, specifically, the XMn₃ family discussed in connection with AHE earlier in this section. It has been shown that the band structure of these materials is nonspin-degenerate, and the direction of the antiferromagnetic order parameter S (defined in Section II) has a well-defined momentum dependence. As a result, the overall conduction across the tunnel barrier can indeed exhibit a dependence on whether the vectors S are aligned parallel or form an angle on two sides of the junction 43,94 . An experimental realization of this effect was observed in two recent works 39,40 , where the material systems chosen were based on PtMn₃ and Mn₃Sn antiferromagnets, respectively, shown in Fig. 8. In both cases, the films were grown epitaxially on non-silicon substrates, and the manipulation of the antiferromagnetic

order was performed by a magnetic field, taking advantage of the finite canted magnetic moment. Even though the manipulation of magnetic order was therefore not electrical, these works point to a promising strategy for fully electrical readout of antiferromagnetic order using TMR in a tunnel junction.

Full antiferromagnetic memory devices such as those shown in Fig. 3, however, will require both electrical reading and writing within the same device structure. While this has not yet been achieved in structures based on fully antiferromagnetic tunnel junctions, another possible strategy is to couple an antiferromagnetic free layer, switched by SOT, to an adjacent ferromagnetic tunnel junction (e.g., based on the widely used CoFeB-MgO material system), and then read it out via ferromagnetic tunneling. This concept, illustrated in Fig. 9, was recently successfully demonstrated ⁶⁰, with the resulting TMR reaching values as high as 80%. However, it is worth noting that some of the challenges associated with ferromagnetic MRAM, such as dipole interaction of neighboring bits, could also be present in arrays made of these hybrid devices.

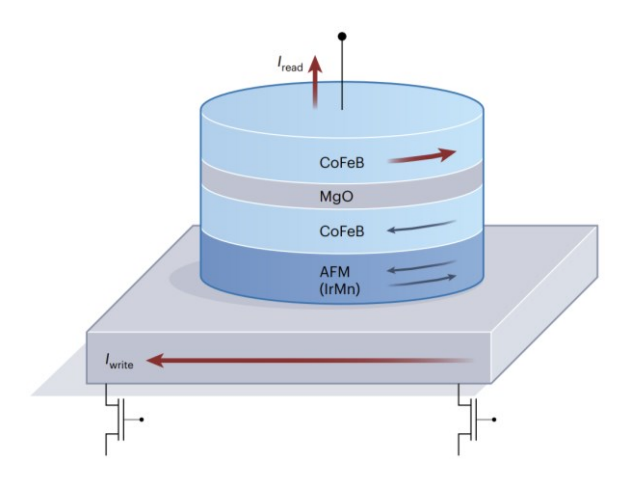


Fig. 9. Illustration of readout of an antiferromagnetic IrMn layer switched by spin-orbit torque, by exchange coupling to a ferromagnetic CoFeB/MgO/CoFeB tunnel junction, as recently demonstrated ⁶⁰. The figure also shows the access transistors that would drive the write current in a typical circuit implementation. Reproduced with permission ⁸⁶.

VI. Imaging of antiferromagnetic domain structures

As previously mentioned, understanding the magnetic domain structure of the Néel vector in

antiferromagnetic materials along with their electrical manipulation can be significantly enhanced by direct imaging approaches. Domains can be described as regions in the material with a uniform order parameter either in orientation or phase. For antiferromagnetic materials, this order parameter is typically the Néel vector. Thus, a sample can have a single domain with uniform Néel vector or can be composed of several domains leading to a domain configuration. Different domains are then separated by a domain wall. The difference between antiferromagnetic domains due to change in the orientation leads to formation of cycloidal or helical states or vortex/anti-vortex states such as those shown in Fig. 5, whereas the difference due to the phase leads to formation of antiphase domains. Furthermore, these changes can be commensurate or incommensurate with respect to the lattice and spin structure. In recent years, there is also increased interest in topology and chirality of the domains such as formation of skyrmions in antiferromagnetic materials. Therefore, understanding the formation, and behavior of domains in antiferromagnetic materials is critical not only from a fundamental standpoint, but also harnessing their properties for spintronic devices. In particular, we need to understand how the domain configuration changes under external stimuli of magnetic field, electric current (e.g., in Fig. 4b) or temperature as well as the effect of local structure and defects on domain behavior. Direct imaging of domains and their behavior in antiferromagnetic materials can provide information which can be coupled with simulations and electrical measurements to form a holistic picture of the dynamics of antiferromagnets.

Imaging of domains in ferromagnets has made tremendous progress over the last several decades, but antiferromagnetic domain imaging has progressed relatively slowly. Direct imaging of antiferromagnetic domains presents several challenges due to the near net-zero magnetization and/or stray field. However, in the recent years, research is ongoing on imaging antiferromagnetic domains with increased spatial and temporal resolution. In the next sections, we will describe the recent capabilities for imaging antiferromagnetic domains, which can be broadly classified into four categories based on the type of probe: (A) Synchrotron X-ray, (B) Electron imaging, (C) Optical imaging, and (D) Scanning probes.

VI.A. Synchrotron X-ray microscopy

Imaging using X-ray magnetic scattering has undergone significant improvement over the past decade due to higher coherence and brightness available at synchrotron sources. X-rays can interact and hence be used to image the magnetic spin textures in antiferromagnetic materials in three possible ways: (1) X-ray scattering effects, (2) X-ray photo emission electron microscopy (PEEM), and (3) coherent Bragg X-ray imaging.

X-ray scattering depends on the photon-spin interaction, which is typically weak compared to Thomson scattering⁹⁵, but with high brightness X-ray photons, it is possible to probe the antiferromagnetic ordered states in materials. The scattering studies can be performed either under resonant conditions or away from resonance. Focusing of the X-rays can be used to spatially probe the local antiferromagnetic order, which was used to image spin density waves in Cr ⁹⁶. The advantage of this approach is that by selecting specific magnetic reflections in q-space, it is possible to image magnetic modulations that break crystal symmetry. Recent work has combined this approach with polarized X-rays to study chiral magnetic scattering such as antiferromagnetic domains with helical modulations, as demonstrated for imaging domains in BiFeO₃ ⁹⁷. Advances in focusing optics have now enabled achieving a spatial resolution down to 50 nm for imaging antiferromagnetic domains.

X-ray PEEM is currently one of the most widely used methods for imaging antiferromagnetic domains with a spatial resolution of 20-30 nm and typically a large field of view ⁹⁸. Linearly polarized X-rays are tuned to the resonance of specific elements and show intensity variations in the near-edge X-ray absorption fine structure in the presence of antiferromagnetic order. Magnetic contrast is then obtained by subtracting signals obtained by changing the direction of polarization parallel and perpendicular to the antiferromagnetic Néel vector ⁹⁹. The electrons emitted in this process are then used to form an image using an electron microscope. This technique is extremely versatile as it provides element specificity, variable depth sensitivity, and allows for separating contributions from various magnetic contributions in multilayer structures or multi-element alloys (Fig. 10a) ^{100, 101}. This method was used to image vortex pairs in antiferromagnetic Fe₂O₃ ¹⁰². Further in-situ experiments are also possible with varying the temperature to as low as 10 K as well as stimuli such as external electric currents and magnetic fields in materials such as CuMnAs (Fig. 10b) ³⁶ and Mn₂Au ¹⁰³. One of

the current limitations of this method is combining with magneto-transport measurements since performing such measurements on antiferromagnetic domains requires significantly large magnetic fields, at which PEEM is difficult to perform.

More recently, coherent X-ray imaging has become popular for high resolution imaging of materials. The advances in detectors and coherence of X-rays enable recording images of speckle patterns in the diffraction plane on the detector and then reconstructing the real-space image using various algorithms such as ptychography. In order to image antiferromagnetic domains, however, it is necessary to be in the magnetic Bragg diffraction geometry ¹⁰⁴. Recent work has shown imaging of antiferromagnetic domain walls in Fe₂Mo₃O₈ using resonant magnetic Bragg diffraction phase contrast ¹⁰⁵.

With better and faster detectors, improved optics, and next-generation X-ray sources, these imaging methods have a bright future to push the resolution to sub-10 nm and image dynamic behavior of antiferromagnetic domains.

VI.B. Electron microscopy

Historically, Lorentz transmission electron microscopy (LTEM) has been used to image domains and domain walls in ferromagnets. The magnetic contrast arises from the electron beam deflection due to the magnetic induction from the sample, or in quantum mechanical terms, the phase shift induced by the sample's vector potential ¹⁰⁶. The magnetic contrast can be observed in out-of-focus images and quantitative information can then be recovered either by phase retrieval approaches ¹⁰⁷ or using methods such as differential phase contrast ^{108, 109} and 4D STEM imaging ¹¹⁰. These approaches have been used for indirect imaging of antiferromagnetic domains through imprinting or interfacing them with ferromagnets. Domain behavior arising from phenomena such as exchange bias between antiferromagnetic materials (IrMn, PtMn) and ferromagnets (NiFe, Fe₃GeTe₂) have been extensively studied using LTEM (see, e.g., Fig. 10c) ¹¹¹⁻¹¹³. Current state-of-art LTEM imaging can achieve sub-nm spatial resolution ¹¹⁴, making it possible to image helical or cycloidal antiferromagnetic order. Similar to X-ray imaging, recent advances in detectors and electron optics have now enabled angstrom scale magnetic imaging where the atomic columns can be resolved along with associated

magnetic fields. Imaging of atomic scale magnetic fields was demonstrated in antiferromagnetic Fe₂O₃ (Fig. 10d), where reorientation of the spin texture because of Morin transition was successfully shown¹¹⁵. Similarly, imaging of atomic scale antiferromagnetic order was also observed in Fe₂As ¹¹⁶. These imaging methods are based on the phase shift associated with the electron wave when it interacts with the magnetic field of the sample. Another method like X-ray dichroism which is based on measuring the electron energy loss spectroscopy and changes in the near-edge structure can also be used to get magnetic information from antiferromagnetic materials. This approach, known as electron magnetic linear dichroism or electron magnetic circular dichroism, can be used to obtain element specific magnetic information in materials such as Fe₂O₃ ¹¹⁷. However, so far this approach is only limited to obtaining spectroscopic signals and only few experiments have been performed to resolve this signal spatially. Future research based on high-quality spectrometers and direct electron detectors should enable spatially resolved imaging of antiferromagnetic order.

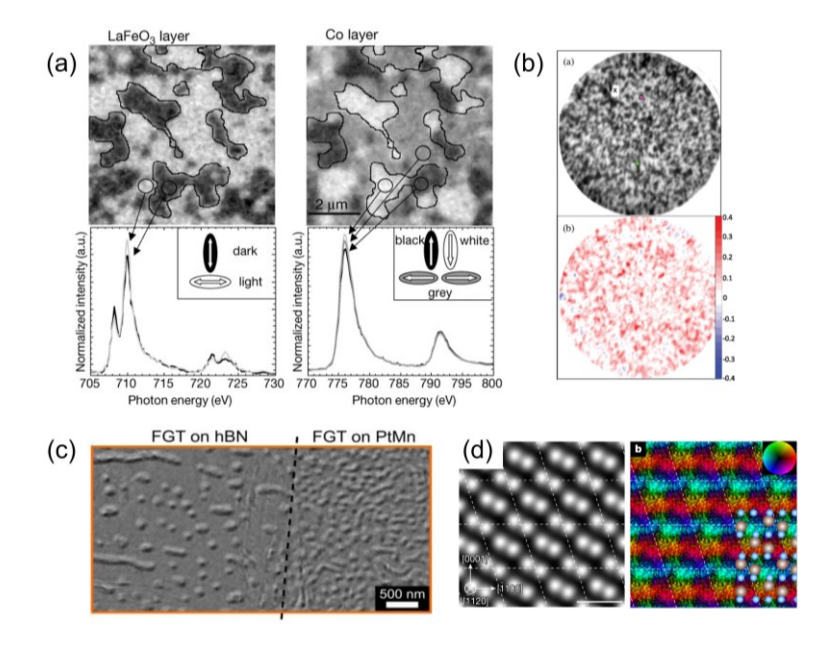


Fig. 10. (a) Correlative imaging of domains and local spectra from antiferromagnetic LaFeO₃ layer and ferromagnetic Co layer obtained using XMLD and XMCD, respectively. Reproduced with permission ¹⁰⁰; (b) XMLD-PEEM image of antiferromagnetic domains in CuMnAs in as grown state and after applying alternate orthogonal current pulse trains. Reproduced with permission ³⁶; (c) Lorentz TEM images of Fe₃GeTe₂ interfaced with hBN and PtMn, showing

difference in domain structure due to interactions with the antiferromagnet. Reproduced with permission ¹¹³; (d) Atomic resolution annular dark field image of Fe₂O₃ and corresponding color map showing the direction of local magnetic induction. Reproduced with permission ¹¹⁵.

VI.C. Optical microscopy

Like transmission electron microscopy, optical microscopy has also been traditionally used for imaging of ferromagnetic domains with sub-micron spatial resolution but significantly higher time resolution. The contrast arises from the magneto-optic Kerr effect (MOKE) which causes the polarization of the reflected light from the surface of the material to be rotated by an angle due to the interaction with the magnetic moment 118, 119. By measuring this change in the polarization, information about the magnetic domains can be obtained. MOKE imaging can be performed in several possible geometries such as polar, longitudinal or transverse, depending on the orientation of the magnetization (perpendicular or parallel to the surface) and the plane of incidence of light. While traditionally, observation of a MOKE signal has been associated with the presence of macroscopic magnetization, in recent years, MOKE imaging has also been extended to image magnetic domains in antiferromagnetic materials. Interestingly, some of the antiferromagnetic materials exhibiting this unconventional optical response are the same ones that exhibit unconventional spin-dependent electrical transport due to their band topology, as discussed in Section V. Domains in non-collinear Mn₃Sn (Fig. 11a) were imaged successfully using MOKE where the signal originated from the ordering of magnetic octupoles (see Section II) in the non-collinear Néel state ⁴⁶. MOKE imaging can also be combined with several in-situ capabilities such as application of external magnetic field, temperature, and electrical biasing to probe the changes in domain structure. This was shown also in Mn_{3+x}Sn_{1-x} films where anomalous Hall effect and MOKE imaging were performed to understand the domain evolution Besides these, MOKE imaging has also been applied for other antiferromagnetic materials such as Mn₂As ¹²¹, Mn₂Au ¹²², and CuMnAs ¹²³. Besides the Kerr effect, another higher order effect known as the magneto-optical birefringence (MOB) effect is also sensitive to the in-plane Néel order in antiferromagnetic materials. The MOB effect exhibits a quadratic dependence on the Néel vector and can be applied to compensated antiferromagnetic materials 124. In addition, imaging of domains can also be performed using a non-linear optical effect known as second harmonic generation (SHG) ¹²⁵. This process involves simultaneous absorption of two photons followed by the emission of a frequency doubled light wave, and typically requires pulsed lasers ¹²⁶. This effect is sensitive to the underlying change in symmetry of the material and hence can be used to detect both ferromagnetic and antiferromagnetic domains. The first example of this technique was demonstrated by imaging antiferromagnetic domains in Cr₂O₃ ¹²⁷. An advantage of SHG is that it can probe coexisting antiferromagnetic sublattices in the material, and their interactions ¹²⁸. SHG has also been used to image domains in antiferromagnetic materials such as MnPS₃ and CrI₃. However, this imaging approach typically requires the use of high-intensity lasers, along with a detailed analysis of the symmetry of the material.

VI.D. Scanning probe microscopy

Unlike the previous imaging techniques, scanning probe microscopy typically involves interaction of a sharp tip with the surface of the sample that is being scanned. Magnetic imaging can be performed using magnetically sensitive probes, which include spin-polarized scanning tunneling microscopy (SP-STM) and magnetic force microscopy (MFM). SP-STM is an extremely powerful technique with atomic resolution to resolve the structure of domain walls and spins on a lattice in antiferromagnetic materials. In SP-STM, the magnetic contrast is based on the spin tunneling current between the spin polarized tip and the sample surface. Pioneering work was done by Bode et. al. on imaging of antiferromagnetic domain wall structure in an ultrathin layer of Fe grown on W. In the recent years, this method has been used to probe the antiferromagnetic domain wall structure in several other antiferromagnetic materials ¹²⁹⁻¹³¹. Most recent work has been performed in combining the SP-STM capability with synchrotron X-rays to obtain simultaneously the magnetic spin information and the local chemical information at atomic resolution ¹³². However, the major limitation of this method is that it requires atomically flat surfaces and due to limited field of view, the domain sizes that can be imaged are relatively small. Magnetic force microscopy depends on the stray field resulting from the magnetic domain structure which acts on the magnetic tip in an atomic force

microscope. In general, for antiferromagnetic materials, there is near zero stray field and hence imaging antiferromagnetic domains using MFM is extremely hard. However, in some cases of non-collinear antiferromagnets or at domain walls with uncompensated spins, it is possible to image them using MFM. This was shown in MnBi₂Te₄ where the antiferromagnetic domain walls show a spin flop state and were successfully imaged below the Néel ordering temperature using cryoMFM (Fig. 11b) ¹³³. There are several modifications of the scanning probe microscopy method available which have been used for imaging antiferromagnetic domains. One such example is scanning nitrogen-vacancy (NV) center microscopy. The NV centers exhibit Zeeman splitting due to the local magnetic field and are extremely sensitive to very small fields at high spatial resolution. This method has been used to image magnetic domains in a variety of antiferromagnetic materials such as Cr₂O₃ ¹³⁴, BiFeO₃ ¹³⁵, and CuCrP₂S₆ ¹³⁶. Other approaches include scanning thermal gradient microscopy where a laser spot is scanned over the surface and the resulting thermo-voltage is recorded 137, magnetic exchange force microscopy which detects the exchange force between the tip and the magnetization on the sample surface ¹³⁸. Scanning probe methods also allow for certain in-situ characterization such as application of magnetic fields, and variation of temperature, but are typically time consuming to acquire the data, and only probe the surface of the sample.

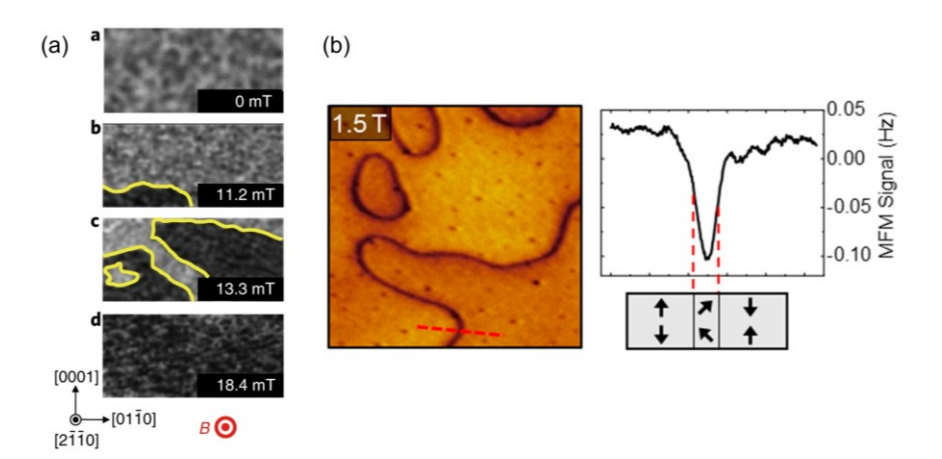


Fig. 11. (a) MOKE images showing evolution of domains as a function of applied magnetic field in the noncollinear antiferromagnetic Mn₃Sn. Reproduced with permission ⁴⁶; (b) MFM image taken at 6 K showing the antiferromagnetic domain wall formed in MnBi_{1.37}Sb_{0.63}Te₄, and the corresponding schematic correlating the MFM signal with the domain wall structure.

VII. Micromagnetic modeling of antiferromagnetic domain structure and dynamics

The information gained from the above-mentioned microscopy approaches, combined with micromagnetic modeling of antiferromagnetic domain structure and dynamics, can enable the antiferromagnetic device research community to achieve more uniform electrically switchable antiferromagnetic states with large on/off ratios, as discussed in Section V. In this section, we provide a brief overview of micromagnetic modeling approaches that have been applied to antiferromagnetic devices.

At the mesoscopic scale, the micromagnetic properties of collinear and non-collinear antiferromagnets can be described by the Landau-Lifshitz-Gilbert (LLG) equation within the two- and three-sublattices model approximation, respectively. Indeed, this implies studying two or three coupled LLG equations, which for the three-sublattice model, can be written as follows.

$$\begin{cases}
\frac{d\mathbf{m}_{1}}{dt} = -\gamma_{0}\mathbf{m}_{1} \times \mathbf{B}_{\text{eff,1}}(\mathbf{m}_{1}, \mathbf{m}_{2}, \mathbf{m}_{3}) + \alpha \mathbf{m}_{1} \times \frac{d\mathbf{m}_{1}}{dt} \\
\frac{d\mathbf{m}_{2}}{dt} = -\gamma_{0}\mathbf{m}_{2} \times \mathbf{B}_{\text{eff,2}}(\mathbf{m}_{1}, \mathbf{m}_{2}, \mathbf{m}_{3}) + \alpha \mathbf{m}_{2} \times \frac{d\mathbf{m}_{2}}{dt} \\
\frac{d\mathbf{m}_{3}}{dt} = -\gamma_{0}\mathbf{m}_{3} \times \mathbf{B}_{\text{eff,3}}(\mathbf{m}_{1}, \mathbf{m}_{2}, \mathbf{m}_{3}) + \alpha \mathbf{m}_{3} \times \frac{d\mathbf{m}_{3}}{dt}
\end{cases} \tag{1}$$

Here, \mathbf{m}_i and $\mathbf{B}_{\text{eff},i}$ (i=1, 2, and 3) are the magnetization vector and the effective magnetic field for the i-th sublattice, respectively. The effective field takes into account all the contributions from external fields, anisotropy, Dzyaloshinskii-Moriya interaction (DMI), and exchange fields ⁸⁸. The equations are coupled through the exchange field which depends on all the three magnetization vectors and for each sublattice is given by five terms, as described below.

$$\mathbf{B}_{1,\text{exch}} = \frac{2A_{11}}{M_S} \nabla^2 \mathbf{m}_1 + \frac{4A_0}{a^2 M_S} \mathbf{m}_2 + \frac{A_{12}}{M_S} \nabla^2 \mathbf{m}_2 + \frac{4A_0}{a^2 M_S} \mathbf{m}_3 + \frac{A_{13}}{M_S} \nabla^2 \mathbf{m}_3,
\mathbf{B}_{2,\text{exch}} = \frac{2A_{22}}{M_S} \nabla^2 \mathbf{m}_2 + \frac{4A_0}{a^2 M_S} \mathbf{m}_3 + \frac{A_{23}}{M_S} \nabla^2 \mathbf{m}_3 + \frac{4A_0}{a^2 M_S} \mathbf{m}_1 + \frac{A_{12}}{M_S} \nabla^2 \mathbf{m}_1,
\mathbf{B}_{3,\text{exch}} = \frac{2A_{33}}{M_S} \nabla^2 \mathbf{m}_3 + \frac{4A_0}{a^2 M_S} \mathbf{m}_1 + \frac{A_{13}}{M_S} \nabla^2 \mathbf{m}_1 + \frac{4A_0}{a^2 M_S} \mathbf{m}_2 + \frac{A_{23}}{M_S} \nabla^2 \mathbf{m}_2.$$
(2)

It can be observed that the exchange field is characterized by two qualitatively different contributions, referred to as homogeneous and non-homogeneous terms. It can be shown that the ground state driven by those terms gives rise to a uniform configuration of \mathbf{m}_i in each

sublattice, the magnetization vector at each different sub-lattice being stabilized in a given plane, set by the magnetic anisotropy of the material, with at rotational angle of 120°. For collinear antiferromagnets, the exchange field has only two contributions and drives a uniform configuration of the magnetization with a configuration where the magnetization vectors are antiparallel, along a direction set by the magnetic anisotropy of the material.

However, as discussed in the previous section, a uniform ground state is rarely observed in magnetic imaging results of antiferromagnets. From a micromagnetic modeling point of view, the key reason can be found in the magnetoelastic interactions of the antiferromagnets with the substate which introduces in the micromagnetic energy landscape a non-uniform magnetic anisotropy. This gives rise to complex domain patterns and/or interesting textures such as magnetic vortex pairs ¹⁰², half skyrmions ¹³⁹ and skyrmions ¹⁴⁰. A remaining challenge is the quantitative micromagnetic modeling of complex magnetic patterns where it is necessary to combine the non-uniform magnetocrystalline anisotropy (grain-dependent value) with the magnetoelastic interactions set by the substrate ^{141, 142}.

As mentioned in Section III, a milestone of antiferromagnetic spintronics was the demonstration of the electrical manipulation of the antiferromagnetic order via current-induced SOT, which is proportional to the current flowing into antiferromagnets for both intrinsic (bulk) SOT effects or to the current flowing into a heavy metal interfaced with the antiferromagnetic layer. In terms of modeling, this SOT can be described by adding an anti-damping term to the LLG equation, similar to the approach used for ferromagnets. This SOT has the same sign in all the sub-lattices and if large enough, can give rise to a net magnetization. This model was successfully used to describe some of the SOT-driven switching experiments in PtMn and IrMn₃ materials ^{25, 26}. In general, this modeling approach also allows the study of nonuniform configurations such as those of Fig. 5, including domain wall dynamics ¹⁴³, which are typically observed in the majority of antiferromagnets.

VIII. Perspectives on device applications

The advances in electrical manipulation and detection of antiferromagnetic order, which were discussed in Sections III to V, open new pathways for the development of a wide range of

potential antiferromagnetic spintronic devices. Among these, we will discuss antiferromagnetic memory and high-frequency (THz) devices as two main examples.

Antiferromagnetic memory devices. The landscape of existing and emerging memory technologies in the semiconductor industry is illustrated in Fig. 12. Overall, it is characterized by a tradeoff between density and speed ^{61, 67, 91, 144, 145}, which can be traced back in part to the electronic interfaces used for each technology, and in part, to the characteristics of the underlying devices. MRAM devices broadly fall within the higher-performance end of this tradeoff, with speed and density that are approximately within the range achievable by static random-access memory (SRAM, which is mostly embedded in logic processes today) and dynamic random-access memory (DRAM, which is mostly implemented in standalone chips, often along with a high-bandwidth memory interface). In ferromagnetic STT-MRAM, achieving higher speed typically requires larger write currents, which in turn reduces the bit density (due to the larger access transistors required) and endurance. Emerging mechanisms such as SOT and VCMA, which are currently moving from research towards development stage, may enable improving this tradeoff by achieving more efficient electrical switching. The newest addition to the family of next-generation MRAM candidates is antiferromagnetic MRAM, which falls within the top right (preferred corner) of this plot. It may, in principle, achieve much higher device-level switching speeds than any of the other emerging MRAM technologies by taking advantage of the exchange-enhanced antiferromagnetic dynamics. It may also achieve high bit density by eliminating bit-to-bit dipole interactions. We hope that the perspectives provided in this article will encourage research on antiferromagnetic device concepts to realize this potential.

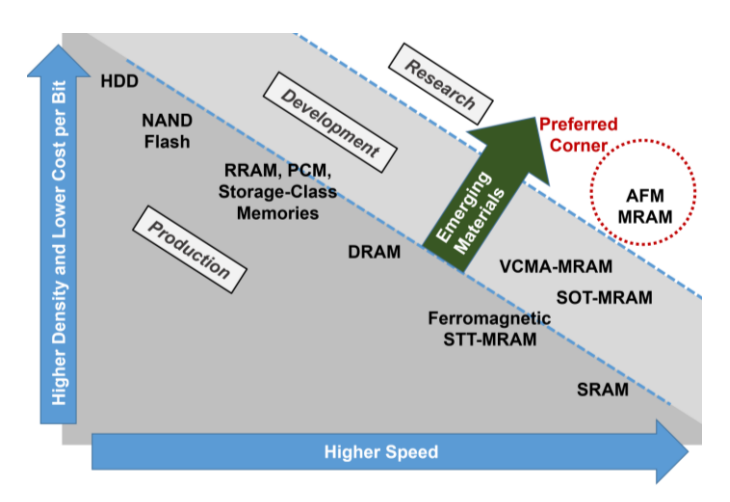


Fig. 12. Overview of incumbent and emerging memory technologies, highlighting their performance-density tradeoff and different stages of development.

Antiferromagnetic THz oscillators and detectors. The manipulation of the antiferromagnetic order driven by SOT also enables a new direction for the application of antiferromagnetic devices for THz technology, a prospect enabled by antiferromagnetic resonances in the THz frequency range. Up to now, the design of these devices has been mainly based on predictions by both analytical and theoretical models, focusing on two possible application categories: Oscillators (sources) and detectors.

Sources of THz radiation based on antiferromagnetic dynamics have been proposed ¹⁴⁶ and studied both analytically and numerically in recent years ^{89, 90, 147}. The main characteristics of these THz oscillators are their room-temperature operation, frequency tunability by electric current and potentially, very high quality factors ⁹⁰. The threshold current in such devices is proportional to the anisotropy field and exhibits a bistability, giving the possibility to sustain the THz dynamics with a current smaller than the threshold current needed to initiate the oscillations. This latter property can result in energy-efficient sources, and may also be useful in the design of spiking neurons. antiferromagnetic oscillators are also expected to exhibit possibilities for frequency modulation and injection locking, which may find applications in communication systems ¹⁴⁸.

Detectors of THz radiation can be presently implemented with various types of photon detectors and thermal detectors (i.e., bolometers), as well as a range of emerging device candidates ¹⁴⁹. Antiferromagnetic THz detectors may offer salient benefits including room-

temperature operation and frequency tunability with current in the passive regime of detection ¹⁵⁰. Emerging principles of detection and manipulation of Néel order, such as the all-antiferromagnetic TMR discussed in Section V, may increase the sensitivity of such antiferromagnetic THz detectors to technologically useful levels. As an example, a recent work predicted that VCMA can parametrically excite the THz response of antiferromagnets with high efficiency and without the need for an external bias field, opening a path to a compact and ultralow power THz technology ⁸⁷.

IX. Summary

The field of antiferromagnetic spintronics is now entering a stage where the tool set of electrically induced torques and magnetoresistance effects is sufficiently developed to begin device-level research for memory, computing, and THz applications. At the same time, there remain many open fundamental questions to be investigated. These range from understanding and utilizing the role of symmetry and topology of antiferromagnetic materials to achieve large electrical detection effects, to investigating the interconnection of such unconventional electrical transport with thermal and optical properties. Other areas of active research will be the improvement of techniques for imaging of antiferromagnetic domain structures, aided by advanced modeling to define strategies for creation of single-domain and textured antiferromagnetic configurations on demand. Coupled with their intrinsic potential technological benefits, including high-frequency dynamics and insensitivity to external fields, this paints a promising perspective for fundamental and applied studies of antiferromagnetic spintronics over the next decade.

Acknowledgements

The work at Northwestern University was supported by the US National Science Foundation through award numbers 2203243, 1853879, and by the National Science Foundation Materials Research Science and Engineering Center at Northwestern University (award number 1720319). The work at Argonne National Laboratory was supported by the US Department of Energy, Office of Science, Office of Basic Energy Sciences, Materials Science and Engineering

Division. The work at the University of Messina was supported by the project PRIN 2020LWPKH7 funded by the Italian Ministry of Universities and Research, and the project No. 101070287 - SWAN-on-chip funded by the European Union within the program HORIZON-CL4-2021-DIGITAL-EMERGING-01.

References

- [1] Wolf, S. A.; Awschalom, D. D.; Buhrman, R. A.; Daughton, J. M.; von Molnár, S.; Roukes, M. L.; Chtchelkanova, A. Y.; Treger, D. M., Spintronics: A Spin-Based Electronics Vision for the Future. *Science* **2001**, *294*, 1488-1495.
- [2] Baibich, M. N.; Broto, J. M.; Fert, A.; Van Dau, F. N.; Petroff, F.; Etienne, P.; Creuzet, G.; Friederich, A.; Chazelas, J., Giant Magnetoresistance of (001)Fe/(001)Cr Magnetic Superlattices. *Physical Review Letters* **1988**, *61*, 2472-2475.
- [3] Binasch, G.; Grünberg, P.; Saurenbach, F.; Zinn, W., Enhanced magnetoresistance in layered magnetic structures with antiferromagnetic interlayer exchange. *Physical Review B* **1989**, *39*, 4828-4830.
- [4] Butler, W. H.; Zhang, X. G.; Schulthess, T. C.; MacLaren, J. M., Spin-dependent tunneling conductance of \$\mathrm{Fe}|\mathrm{MgO}|\mathrm{Fe}\$ sandwiches. *Physical Review B* **2001**, *63*, 054416.
- [5] Yuasa, S.; Nagahama, T.; Fukushima, A.; Suzuki, Y.; Ando, K., Giant room-temperature magnetoresistance in single-crystal Fe/MgO/Fe magnetic tunnel junctions. *Nature Materials* **2004**, *3*, 868-871.
- [6] Parkin, S. S. P.; Kaiser, C.; Panchula, A.; Rice, P. M.; Hughes, B.; Samant, M.; Yang, S.-H., Giant tunnelling magnetoresistance at room temperature with MgO (100) tunnel barriers. *Nature Materials* **2004**, *3*, 862-867.
- [7] Slonczewski, J. C., Current-driven excitation of magnetic multilayers. *Journal of Magnetism and Magnetic Materials* **1996**, *159*, L1-L7.
- [8] Katine, J. A.; Albert, F. J.; Buhrman, R. A.; Myers, E. B.; Ralph, D. C., Current-Driven Magnetization Reversal and Spin-Wave Excitations in Co/Cu/Co Pillars. *Physical Review Letters* **2000**, *84*, 3149-3152.
- [9] Miron, I. M.; Garello, K.; Gaudin, G.; Zermatten, P.-J.; Costache, M. V.; Auffret, S.; Bandiera, S.; Rodmacq, B.; Schuhl, A.; Gambardella, P., Perpendicular switching of a single ferromagnetic layer induced by in-plane current injection. *Nature* **2011**, *476*, 189-193.
- [10] Liu, L.; Pai, C.-F.; Li, Y.; Tseng, H. W.; Ralph, D. C.; Buhrman, R. A., Spin-Torque Switching with the Giant Spin Hall Effect of Tantalum. *Science* **2012**, *336*, 555-558.
- [11] Chiba, D.; Fukami, S.; Shimamura, K.; Ishiwata, N.; Kobayashi, K.; Ono, T., Electrical control of the ferromagnetic phase transition in cobalt at room temperature. *Nature Materials* **2011**, *10*, 853-856.
- [12] Shiota, Y.; Nozaki, T.; Bonell, F.; Murakami, S.; Shinjo, T.; Suzuki, Y., Induction of coherent magnetization switching in a few atomic layers of FeCo using voltage pulses. *Nat Mater* **2012**, *11*, 39-43.
- [13] Wang, W.-G.; Li, M.; Hageman, S.; Chien, C. L., Electric-field-assisted switching in magnetic

- tunnel junctions. Nature Materials 2012, 11, 64.
- [14] Zhu, J.; Katine, J. A.; Rowlands, G. E.; Chen, Y.-J.; Duan, Z.; Alzate, J. G.; Upadhyaya, P.; Langer, J.; Amiri, P. K.; Wang, K. L.; Krivorotov, I. N., Voltage-Induced Ferromagnetic Resonance in Magnetic Tunnel Junctions. *Physical Review Letters* **2012**, *108*, 197203.
- [15] Cherepov, S.; Amiri, P. K.; Alzate, J. G.; Wong, K.; Lewis, M.; Upadhyaya, P.; Nath, J.; Bao, M.; Bur, A.; Wu, T.; Carman, G. P.; Khitun, A.; Wang, K. L., Electric-field-induced spin wave generation using multiferroic magnetoelectric cells. *Applied Physics Letters* **2014**, *104*, 082403.
- [16] Wu, T.; Bur, A.; Wong, K.; Zhao, P.; Lynch, C. S.; Amiri, P. K.; Wang, K. L.; Carman, G. P., Electrical control of reversible and permanent magnetization reorientation for magnetoelectric memory devices. *Applied Physics Letters* **2011**, *98*, 262504.
- [17] Kent, A. D.; Worledge, D. C., A new spin on magnetic memories. *Nature Nanotechnology* **2015**, *10*, 187.
- [18] Wang, K. L.; Alzate, J. G.; Khalili Amiri, P., Low-power non-volatile spintronic memory: STT-RAM and beyond. *Journal of Physics D: Applied Physics* **2013**, *46*, 074003.
- [19] Zhang, L.; Fang, B.; Cai, J.; Carpentieri, M.; Puliafito, V.; Garesci, F.; Amiri, P. K.; Finocchio, G.; Zeng, Z., Ultrahigh detection sensitivity exceeding 10⁵ V/W in spin-torque diode. *Applied Physics Letters* **2018**, *113*, 102401.
- [20] Fang, B.; Carpentieri, M.; Hao, X.; Jiang, H.; Katine, J. A.; Krivorotov, I. N.; Ocker, B.; Langer, J.; Wang, K. L.; Zhang, B.; Azzerboni, B.; Amiri, P. K.; Finocchio, G.; Zeng, Z., Giant spin-torque diode sensitivity in the absence of bias magnetic field. *Nature Communications* **2016**, *7*, 11259.
- [21] Fang, B.; Carpentieri, M.; Louis, S.; Tiberkevich, V.; Slavin, A.; Krivorotov, I. N.; Tomasello, R.; Giordano, A.; Jiang, H.; Cai, J.; Fan, Y.; Zhang, Z.; Zhang, B.; Katine, J. A.; Wang, K. L.; Amiri, P. K.; Finocchio, G.; Zeng, Z., Experimental Demonstration of Spintronic Broadband Microwave Detectors and Their Capability for Powering Nanodevices. *Physical Review Applied* **2019**, *11*, 014022.
- [22] Zeng, Z.; Finocchio, G.; Zhang, B.; Amiri, P. K.; Katine, J. A.; Krivorotov, I. N.; Huai, Y.; Langer, J.; Azzerboni, B.; Wang, K. L.; Jiang, H., Ultralow-current-density and bias-field-free spin-transfer nano-oscillator. *Scientific Reports* **2013**, *3*, 1426.
- [23] Zeng, Z.; Amiri, P. K.; Krivorotov, I. N.; Zhao, H.; Finocchio, G.; Wang, J.-P.; Katine, J. A.; Huai, Y.; Langer, J.; Galatsis, K.; Wang, K. L.; Jiang, H., High-Power Coherent Microwave Emission from Magnetic Tunnel Junction Nano-oscillators with Perpendicular Anisotropy. *ACS Nano* **2012**, *6*, 6115-6121.
- [24] Neel, L., Magnetism and the Local Molecular Field. Nobel Lecture 1970.
- [25] Arpaci, S.; Lopez-Dominguez, V.; Shi, J.; Sánchez-Tejerina, L.; Garesci, F.; Wang, C.; Yan, X.; Sangwan, V. K.; Grayson, M. A.; Hersam, M. C.; Finocchio, G.; Khalili Amiri, P., Observation of current-induced switching in non-collinear antiferromagnetic IrMn3 by differential voltage measurements. *Nature Communications* **2021**, *12*, 3828.
- [26] Shi, J.; Lopez-Dominguez, V.; Garesci, F.; Wang, C.; Almasi, H.; Grayson, M.; Finocchio, G.; Khalili Amiri, P., Electrical manipulation of the magnetic order in antiferromagnetic PtMn pillars. *Nature Electronics* **2020**.
- [27] DuttaGupta, S.; Kurenkov, A.; Tretiakov, O. A.; Krishnaswamy, G.; Sala, G.; Krizakova, V.; Maccherozzi, F.; Dhesi, S. S.; Gambardella, P.; Fukami, S.; Ohno, H., Spin-orbit torque switching of an antiferromagnetic metallic heterostructure. *Nature Communications* **2020**, *11*, 5715.

- [28] Cheng, Y.; Yu, S.; Zhu, M.; Hwang, J.; Yang, F., Electrical Switching of Tristate Antiferromagnetic Neel Order in alpha-Fe2O3 Epitaxial Films. *Physical Review Letters* **2020**, *124*, 027202.
- [29] Olejník, K.; Seifert, T.; Kašpar, Z.; Novák, V.; Wadley, P.; Campion Richard, P.; Baumgartner, M.; Gambardella, P.; Němec, P.; Wunderlich, J.; Sinova, J.; Kužel, P.; Müller, M.; Kampfrath, T.; Jungwirth, T., Terahertz electrical writing speed in an antiferromagnetic memory. *Science Advances* **2018**, *4*, eaar3566.
- [30] Jungfleisch, M. B.; Zhang, W.; Hoffmann, A., Perspectives of antiferromagnetic spintronics. *Physics Letters A* **2018**, *382*, 865-871.
- [31] Moriyama, T.; Oda, K.; Ohkochi, T.; Kimata, M.; Ono, T., Spin torque control of antiferromagnetic moments in NiO. *Scientific Reports* **2018**, *8*, 14167.
- [32] Godinho, J.; Reichlová, H.; Kriegner, D.; Novák, V.; Olejník, K.; Kašpar, Z.; Šobáň, Z.; Wadley, P.; Campion, R. P.; Otxoa, R. M.; Roy, P. E.; Železný, J.; Jungwirth, T.; Wunderlich, J., Electrically induced and detected Néel vector reversal in a collinear antiferromagnet. *Nature Communications* **2018**, *9*, 4686.
- [33] Bodnar, S. Y.; Šmejkal, L.; Turek, I.; Jungwirth, T.; Gomonay, O.; Sinova, J.; Sapozhnik, A. A.; Elmers, H. J.; Kläui, M.; Jourdan, M., Writing and reading antiferromagnetic Mn2Au by Néel spin-orbit torques and large anisotropic magnetoresistance. *Nature Communications* **2018**, *9*, 348.
- [34] Liu, Z. Q.; Chen, H.; Wang, J. M.; Liu, J. H.; Wang, K.; Feng, Z. X.; Yan, H.; Wang, X. R.; Jiang, C. B.; Coey, J. M. D.; MacDonald, A. H., Electrical switching of the topological anomalous Hall effect in a non-collinear antiferromagnet above room temperature. *Nature Electronics* **2018**, *1*, 172-177.
- [35] Olejník, K.; Schuler, V.; Marti, X.; Novák, V.; Kašpar, Z.; Wadley, P.; Campion, R. P.; Edmonds, K. W.; Gallagher, B. L.; Garces, J.; Baumgartner, M.; Gambardella, P.; Jungwirth, T., Antiferromagnetic CuMnAs multi-level memory cell with microelectronic compatibility. *Nature Communications* **2017**, *8*, 15434.
- [36] Grzybowski, M. J.; Wadley, P.; Edmonds, K. W.; Beardsley, R.; Hills, V.; Campion, R. P.; Gallagher, B. L.; Chauhan, J. S.; Novak, V.; Jungwirth, T.; Maccherozzi, F.; Dhesi, S. S., Imaging Current-Induced Switching of Antiferromagnetic Domains in CuMnAs. *Physical Review Letters* **2017**, *118*, 057701.
- [37] Wadley, P.; Howells, B.; Železný, J.; Andrews, C.; Hills, V.; Campion, R. P.; Novák, V.; Olejník, K.; Maccherozzi, F.; Dhesi, S. S.; Martin, S. Y.; Wagner, T.; Wunderlich, J.; Freimuth, F.; Mokrousov, Y.; Kuneš, J.; Chauhan, J. S.; Grzybowski, M. J.; Rushforth, A. W.; Edmonds, K. W.; Gallagher, B. L.; Jungwirth, T., Electrical switching of an antiferromagnet. *Science* **2016**, *351*, 587-590.
- [38] Jungwirth, T.; Marti, X.; Wadley, P.; Wunderlich, J., Antiferromagnetic spintronics. *Nature Nanotechnology* **2016**, *11*, 231-241.
- [39] Chen, X.; Higo, T.; Tanaka, K.; Nomoto, T.; Tsai, H.; Idzuchi, H.; Shiga, M.; Sakamoto, S.; Ando, R.; Kosaki, H.; Matsuo, T.; Nishio-Hamane, D.; Arita, R.; Miwa, S.; Nakatsuji, S., Octupole-driven magnetoresistance in an antiferromagnetic tunnel junction. *Nature* **2023**, *613*, 490-495.
- [40] Qin, P.; Yan, H.; Wang, X.; Chen, H.; Meng, Z.; Dong, J.; Zhu, M.; Cai, J.; Feng, Z.; Zhou, X.; Liu, L.; Zhang, T.; Zeng, Z.; Zhang, J.; Jiang, C.; Liu, Z., Room-temperature

- magnetoresistance in an all-antiferromagnetic tunnel junction. Nature 2023, 613, 485-489.
- [41] Ghosh, S.; Manchon, A.; Železný, J., Unconventional Robust Spin-Transfer Torque in Noncollinear Antiferromagnetic Junctions. *Physical Review Letters* **2022**, *128*, 097702.
- [42] Bose, A.; Schreiber, N. J.; Jain, R.; Shao, D.-F.; Nair, H. P.; Sun, J.; Zhang, X. S.; Muller, D. A.; Tsymbal, E. Y.; Schlom, D. G.; Ralph, D. C., Tilted spin current generated by the collinear antiferromagnet ruthenium dioxide. *Nature Electronics* **2022**, *5*, 267-274.
- [43] Dong, J.; Li, X.; Gurung, G.; Zhu, M.; Zhang, P.; Zheng, F.; Tsymbal, E. Y.; Zhang, J., Tunneling Magnetoresistance in Noncollinear Antiferromagnetic Tunnel Junctions. *Physical Review Letters* **2022**, *128*, 197201.
- [44] Siddiqui, S. A.; Sklenar, J.; Kang, K.; Gilbert, M. J.; Schleife, A.; Mason, N.; Hoffmann, A., Metallic antiferromagnets. *Journal of Applied Physics* **2020**, *128*, 040904.
- [45] Ghimire, N. J.; Botana, A. S.; Jiang, J. S.; Zhang, J.; Chen, Y. S.; Mitchell, J. F., Large anomalous Hall effect in the chiral-lattice antiferromagnet CoNb3S6. *Nature Communications* **2018**, *9*, 3280.
- [46] Higo, T.; Man, H.; Gopman, D. B.; Wu, L.; Koretsune, T.; van 't Erve, O. M. J.; Kabanov, Y. P.; Rees, D.; Li, Y.; Suzuki, M.-T.; Patankar, S.; Ikhlas, M.; Chien, C. L.; Arita, R.; Shull, R. D.; Orenstein, J.; Nakatsuji, S., Large magneto-optical Kerr effect and imaging of magnetic octupole domains in an antiferromagnetic metal. *Nature Photonics* **2018**, *12*, 73-78.
- [47] Šmejkal, L.; Mokrousov, Y.; Yan, B.; MacDonald, A. H., Topological antiferromagnetic spintronics. *Nature Physics* **2018**, *14*, 242-251.
- [48] Ikhlas, M.; Tomita, T.; Koretsune, T.; Suzuki, M.-T.; Nishio-Hamane, D.; Arita, R.; Otani, Y.; Nakatsuji, S., Large anomalous Nernst effect at room temperature in a chiral antiferromagnet. *Nature Physics* **2017**, *13*, 1085-1090.
- [49] Železný, J.; Zhang, Y.; Felser, C.; Yan, B., Spin-Polarized Current in Noncollinear Antiferromagnets. *Physical Review Letters* **2017**, *119*, 187204.
- [50] Nakatsuji, S.; Kiyohara, N.; Higo, T., Large anomalous Hall effect in a non-collinear antiferromagnet at room temperature. *Nature* **2015**, *527*, 212-215.
- [51] Chen, H.; Niu, Q.; MacDonald, A. H., Anomalous Hall Effect Arising from Noncollinear Antiferromagnetism. *Physical Review Letters* **2014**, *112*, 017205.
- [52] Kübler, J.; Felser, C., Non-collinear antiferromagnets and the anomalous Hall effect. *EPL (Europhysics Letters)* **2014**, *108*, 67001.
- [53] Šmejkal, L.; Sinova, J.; Jungwirth, T., Emerging Research Landscape of Altermagnetism. *Physical Review X* **2022**, *12*, 040501.
- [54] Šmejkal, L.; González-Hernández, R.; Jungwirth, T.; Sinova, J., Crystal time-reversal symmetry breaking and spontaneous Hall effect in collinear antiferromagnets. *Science Advances* **2020**, *6*, eaaz8809.
- [55] Go, D.; Sallermann, M.; Lux, F. R.; Blügel, S.; Gomonay, O.; Mokrousov, Y., Noncollinear Spin Current for Switching of Chiral Magnetic Textures. *Physical Review Letters* **2022**, *129*, 097204.
- [56] Yamane, Y.; Gomonay, O.; Sinova, J., Dynamics of noncollinear antiferromagnetic textures driven by spin current injection. *Physical Review B* **2019**, *100*, 054415.
- [57] Gomonaj, E. V.; L'Vov, V. A., Phenomenologic study of phase transitions in noncollinear antiferromagnets of metallic perovskite type. *Phase Transitions* **1992**, *38*, 15-31.
- [58] Tsai, H.; Higo, T.; Kondou, K.; Nomoto, T.; Sakai, A.; Kobayashi, A.; Nakano, T.; Yakushiji, K.; Arita, R.; Miwa, S.; Otani, Y.; Nakatsuji, S., Electrical manipulation of a

- topological antiferromagnetic state. Nature 2020, 580, 608-613.
- [59] Železný, J.; Wadley, P.; Olejník, K.; Hoffmann, A.; Ohno, H., Spin transport and spin torque in antiferromagnetic devices. *Nature Physics* **2018**, *14*, 220-228.
- [60] Du, A.; Zhu, D.; Cao, K.; Zhang, Z.; Guo, Z.; Shi, K.; Xiong, D.; Xiao, R.; Cai, W.; Yin, J.; Lu, S.; Zhang, C.; Zhang, Y.; Luo, S.; Fert, A.; Zhao, W., Electrical manipulation and detection of antiferromagnetism in magnetic tunnel junctions. *Nature Electronics* **2023**.
- [61] Lopez-Dominguez, V.; Shao, Y.; Khalili Amiri, P., Perspectives on field-free spin—orbit torque devices for memory and computing applications. *Journal of Applied Physics* **2023**, *133*, 040902.
- [62] Chiang, C. C.; Huang, S. Y.; Qu, D.; Wu, P. H.; Chien, C. L., Absence of Evidence of Electrical Switching of the Antiferromagnetic N\'eel Vector. *Physical Review Letters* **2019**, *123*, 227203.
- [63] Shi, J. Antiferromagnetic spin-orbit torque devices for random-access memory applications. Northwestern University, 2023.
- [64] Zheng, Z.; Zhang, Y.; Lopez-Dominguez, V.; Sánchez-Tejerina, L.; Shi, J.; Feng, X.; Chen, L.; Wang, Z.; Zhang, Z.; Zhang, K.; Hong, B.; Xu, Y.; Zhang, Y.; Carpentieri, M.; Fert, A.; Finocchio, G.; Zhao, W.; Khalili Amiri, P., Field-free spin-orbit torque-induced switching of perpendicular magnetization in a ferrimagnetic layer with a vertical composition gradient. *Nature Communications* **2021**, *12*, 4555.
- [65] Yu, G.; Upadhyaya, P.; Fan, Y.; Alzate, J. G.; Jiang, W.; Wong, K. L.; Takei, S.; Bender, S. A.; Chang, L.-T.; Jiang, Y.; Lang, M.; Tang, J.; Wang, Y.; Tserkovnyak, Y.; Khalili Amiri, P.; Wang, K. L., Switching of perpendicular magnetization by spin—orbit torques in the absence of external magnetic fields. *Nature Nanotechnology* **2014**, *9*, 548-554.
- [66] Nozaki, T.; Yamamoto, T.; Miwa, S.; Tsujikawa, M.; Shirai, M.; Yuasa, S.; Suzuki, Y., Recent Progress in the Voltage-Controlled Magnetic Anisotropy Effect and the Challenges Faced in Developing Voltage-Torque MRAM. *Micromachines* **2019**, *10*.
- [67] Shao, Y.; Khalili Amiri, P., Progress and Application Perspectives of Voltage-Controlled Magnetic Tunnel Junctions. *Advanced Materials Technologies* **2023**, *n/a*, 2300676.
- [68] Grezes, C.; Ebrahimi, F.; Alzate, J. G.; Cai, X.; Katine, J. A.; Langer, J.; Ocker, B.; Amiri, P. K.; Wang, K. L., Ultra-low switching energy and scaling in electric-field-controlled nanoscale magnetic tunnel junctions with high resistance-area product. *Applied Physics Letters* **2016**, *108*, 012403.
- [69] Amiri, P. K.; Alzate, J. G.; Cai, X. Q.; Ebrahimi, F.; Hu, Q.; Wong, K.; Grèzes, C.; Lee, H.; Yu, G.; Li, X.; Akyol, M.; Shao, Q.; Katine, J. A.; Langer, J.; Ocker, B.; Wang, K. L., Electric-Field-Controlled Magnetoelectric RAM: Progress, Challenges, and Scaling. *IEEE Transactions on Magnetics* **2015**, *51*, 1-7.
- [70] Shao, Y.; Lopez-Dominguez, V.; Davila, N.; Sun, Q.; Kioussis, N.; Katine, J. A.; Khalili Amiri, P., Sub-volt switching of nanoscale voltage-controlled perpendicular magnetic tunnel junctions. *Communications Materials* **2022**, *3*, 87.
- [71] Khalili Amiri, P.; Wang, K. L., Voltage-controlled magnetic anisotropy in spintronic devices. *SPIN* **2012**, *02*, 1240002.
- [72] Worledge, D. C.; Hu, G.; Abraham, D. W.; Sun, J. Z.; Trouilloud, P. L.; Nowak, J.; Brown, S.; Gaidis, M. C.; O'Sullivan, E. J.; Robertazzi, R. P., Spin torque switching of perpendicular Ta|CoFeB|MgO-based magnetic tunnel junctions. *Applied Physics Letters* **2011**, *98*, 022501.
- [73] Ikeda, S.; Miura, K.; Yamamoto, H.; Mizunuma, K.; Gan, H. D.; Endo, M.; Kanai, S.; Hayakawa, J.; Matsukura, F.; Ohno, H., A perpendicular-anisotropy CoFeB–MgO magnetic tunnel

- junction. Nature Materials 2010, 9, 721-724.
- [74] Khalili Amiri, P.; Zeng, Z. M.; Langer, J.; Zhao, H.; Rowlands, G.; Chen, Y. J.; Krivorotov, I. N.; Wang, J. P.; Jiang, H. W.; Katine, J. A.; Huai, Y.; Galatsis, K.; Wang, K. L., Switching current reduction using perpendicular anisotropy in CoFeB–MgO magnetic tunnel junctions. *Applied Physics Letters* **2011**, *98*, 112507.
- [75] Shao, Y.; Duffee, C.; Raimondo, E.; Davila, N.; Lopez-Dominguez, V.; Katine, J.; Finocchio, G.; Khalili, P., Probabilistic computing with voltage-controlled dynamics in magnetic tunnel junctions. *Nanotechnology* **2023**.
- [76] Shao, Y.; Davila, N.; Ebrahimi, F.; Katine, J. A.; Finocchio, G.; Khalili Amiri, P., Reconfigurable Physically Unclonable Functions Based on Nanoscale Voltage-Controlled Magnetic Tunnel Junctions. *Advanced Electronic Materials* **2023**, *9*, 2300195.
- [77] Lee, H.; Ebrahimi, F.; Amiri, P. K.; Wang, K. L., Design of high-throughput and low-power true random number generator utilizing perpendicularly magnetized voltage-controlled magnetic tunnel junction. *AIP Advances* **2017**, *7*, 055934.
- [78] Bhattacharya, D.; Razavi, S. A.; Wu, H.; Dai, B.; Wang, K. L.; Atulasimha, J., Creation and annihilation of non-volatile fixed magnetic skyrmions using voltage control of magnetic anisotropy. *Nature Electronics* **2020**, *3*, 539-545.
- [79] Upadhyaya, P.; Yu, G.; Amiri, P. K.; Wang, K. L., Electric-field guiding of magnetic skyrmions. *Physical Review B* **2015**, *92*, 134411.
- [80] Schroeter, S.; Garst, M., Scattering of high-energy magnons off a magnetic skyrmion. *Low Temperature Physics* **2015**, *41*, 817-825.
- [81] Schütte, C.; Garst, M., Magnon-skyrmion scattering in chiral magnets. *Physical Review B* **2014**, *90*, 094423.
- [82] Hu, Z.; Shao, Y.; Lopez-Dominguez, V.; Amiri, P. K., Micromagnetic Investigation of a Voltage-Controlled Skyrmionic Magnon Switch. *Physical Review Applied* **2022**, *17*, 044055.
- [83] Zheng, G.; Ke, S.-H.; Miao, M.; Kim, J.; Ramesh, R.; Kioussis, N., Electric field control of magnetization direction across the antiferromagnetic to ferromagnetic transition. *Scientific Reports* **2017**, *7*, 5366.
- [84] Chang, P. H.; Fang, W.; Ozaki, T.; Belashchenko, K. D., Voltage-controlled magnetic anisotropy in antiferromagnetic MgO-capped MnPt films. *Physical Review Materials* **2021**, *5*, 054406.
- [85] Lopez-Dominguez, V.; Almasi, H.; Khalili Amiri, P., Picosecond Electric-Field-Induced Switching of Antiferromagnets. *Physical Review Applied* **2019**, *11*, 024019.
- [86] Khalili Amiri, P.; Garesci, F.; Finocchio, G., Current-controlled antiferromagnetic memory. *Nature Electronics* **2023**.
- [87] Tomasello, R.; Verba, R.; Lopez-Dominguez, V.; Garesci, F.; Carpentieri, M.; Di Ventra, M.; Khalili Amiri, P.; Finocchio, G., Antiferromagnetic Parametric Resonance Driven by Voltage-Controlled Magnetic Anisotropy. *Physical Review Applied* **2022**, *17*, 034004.
- [88] Tomasello, R.; Sanchez-Tejerina, L.; Lopez-Dominguez, V.; Garesci, F.; Giordano, A.; Carpentieri, M.; Khalili Amiri, P.; Finocchio, G., Domain periodicity in an easy-plane antiferromagnet with Dzyaloshinskii-Moriya interaction. *Physical Review B* **2020**, *102*, 224432.
- [89] Puliafito, V.; Khymyn, R.; Carpentieri, M.; Azzerboni, B.; Tiberkevich, V.; Slavin, A.; Finocchio, G., Micromagnetic modeling of terahertz oscillations in an antiferromagnetic material driven by the spin Hall effect. *Physical Review B* **2019**, *99*, 024405.
- [90] Khymyn, R.; Lisenkov, I.; Tiberkevich, V.; Ivanov, B. A.; Slavin, A., Antiferromagnetic THz-

- frequency Josephson-like Oscillator Driven by Spin Current. Scientific Reports 2017, 7, 43705.
- [91] Finocchio, G.; Di Ventra, M.; Camsari, K. Y.; Everschor-Sitte, K.; Khalili Amiri, P.; Zeng, Z., The promise of spintronics for unconventional computing. *Journal of Magnetism and Magnetic Materials* **2021**, *521*, 167506.
- [92] Mazin, I.; The, P. R. X. E., Editorial: Altermagnetism---A New Punch Line of Fundamental Magnetism. *Physical Review X* **2022**, *12*, 040002.
- [93] Shao, D.-F.; Zhang, S.-H.; Li, M.; Eom, C.-B.; Tsymbal, E. Y., Spin-neutral currents for spintronics. *Nature Communications* **2021**, *12*, 7061.
- [94] Nan, T.; Quintela, C. X.; Irwin, J.; Gurung, G.; Shao, D. F.; Gibbons, J.; Campbell, N.; Song, K.; Choi, S. Y.; Guo, L.; Johnson, R. D.; Manuel, P.; Chopdekar, R. V.; Hallsteinsen, I.; Tybell, T.; Ryan, P. J.; Kim, J. W.; Choi, Y.; Radaelli, P. G.; Ralph, D. C.; Tsymbal, E. Y.; Rzchowski, M. S.; Eom, C. B., Controlling spin current polarization through non-collinear antiferromagnetism. *Nature Communications* **2020**, *11*, 4671.
- [95] Brunel, M.; de Bergevin, F., Diffraction of X-rays by magnetic materials. II. Measurements on antiferromagnetic Fe2O3. *Acta Crystallographica Section A* **1981**, *37*, 324-331.
- [96] Evans, P. G.; Isaacs, E. D.; Aeppli, G.; Cai, Z.; Lai, B., X-ray Microdiffraction Images of Antiferromagnetic Domain Evolution in Chromium. *Science* **2002**, *295*, 1042-1045.
- [97] Johnson, R. D.; Barone, P.; Bombardi, A.; Bean, R. J.; Picozzi, S.; Radaelli, P. G.; Oh, Y. S.; Cheong, S. W.; Chapon, L. C., X-Ray Imaging and Multiferroic Coupling of Cycloidal Magnetic Domains in Ferroelectric Monodomain BiFeO3. *Physical Review Letters* **2013**, *110*, 217206.
- [98] Stöhr, J.; Scholl, A.; Regan, T. J.; Anders, S.; Lüning, J.; Scheinfein, M. R.; Padmore, H. A.; White, R. L., Images of the Antiferromagnetic Structure of a NiO(100) Surface by Means of X-Ray Magnetic Linear Dichroism Spectromicroscopy. *Physical Review Letters* **1999**, *83*, 1862-1865.
- [99] Stöhr, J.; Padmore, H. A.; Anders, S.; Stammler, T.; Scheinfein, M. R., Principles of X-Ray Magnetic Dichroism Spectromicroscopy. *Surface Review and Letters* **1998**, *05*, 1297-1308.
- [100] Nolting, F.; Scholl, A.; Stöhr, J.; Seo, J. W.; Fompeyrine, J.; Siegwart, H.; Locquet, J. P.; Anders, S.; Lüning, J.; Fullerton, E. E.; Toney, M. F.; Scheinfein, M. R.; Padmore, H. A., Direct observation of the alignment of ferromagnetic spins by antiferromagnetic spins. *Nature* **2000**, *405*, 767-769.
- [101] Ohldag, H.; Scholl, A.; Nolting, F.; Anders, S.; Hillebrecht, F. U.; Stöhr, J., Spin Reorientation at the Antiferromagnetic NiO(001) Surface in Response to an Adjacent Ferromagnet. *Physical Review Letters* **2001**, *86*, 2878-2881.
- [102] Chmiel, F. P.; Waterfield Price, N.; Johnson, R. D.; Lamirand, A. D.; Schad, J.; van der Laan, G.; Harris, D. T.; Irwin, J.; Rzchowski, M. S.; Eom, C. B.; Radaelli, P. G., Observation of magnetic vortex pairs at room temperature in a planar α-Fe2O3/Co heterostructure. *Nature Materials* **2018**, *17*, 581-585.
- [103] Sapozhnik, A. A.; Filianina, M.; Bodnar, S. Y.; Lamirand, A.; Mawass, M. A.; Skourski, Y.; Elmers, H. J.; Zabel, H.; Kläui, M.; Jourdan, M., Direct imaging of antiferromagnetic domains in ${\mathbf{Mn}}_{2}\$ mathrm {Au} manipulated by high magnetic fields. *Physical Review B* **2018**, *97*, 134429.
- [104] Bluschke, M.; Basak, R.; Barbour, A.; Warner, A. N.; Fürsich, K.; Wilkins, S.; Roy, S.; Lee, J.; Christiani, G.; Logvenov, G.; Minola, M.; Keimer, B.; Mazzoli, C.; Benckiser, E.; Frano, A., Imaging mesoscopic antiferromagnetic spin textures in the dilute limit from single-geometry resonant coherent x-ray diffraction. *Science Advances* 8, eabn6882.

- [105] Kim, M. G.; Miao, H.; Gao, B.; Cheong, S. W.; Mazzoli, C.; Barbour, A.; Hu, W.; Wilkins, S. B.; Robinson, I. K.; Dean, M. P. M.; Kiryukhin, V., Imaging antiferromagnetic antiphase domain boundaries using magnetic Bragg diffraction phase contrast. *Nature Communications* **2018**, *9*, 5013.
- [106] Petford-Long, A. K.; De Graef, M., In *Characterization of Materials*, John Wiley & Sons, Inc.: Hoboken, NJ, USA, 2012; pp 1-15.
- [107] Phatak, C.; De Graef, M., In *Mesoscopic Phenomenon in Multifunctional Materials*, Saxena, A.; Planes, A., Eds. Springer: Berlin, 2014; pp 137–158.
- [108] Chapman, J. N.; Ploessl, R.; Donnet, D. M., Differential phase contrast microscopy of magnetic materials. *Ultramicroscopy* **1992**, *47*, 331-338.
- [109] Lubk, A.; Zweck, J., Differential phase contrast: An integral perspective. *Physical Review A* **2015**, *91*, 023805.
- [110] Ophus, C., Four-Dimensional Scanning Transmission Electron Microscopy (4D-STEM): From Scanning Nanodiffraction to Ptychography and Beyond. *Microscopy and Microanalysis* **2019**, *25*, 563-582.
- [111] Tanase, M.; Petford-Long, A. K.; Heinonen, O.; Buchanan, K. S.; Sort, J.; Nogués, J., Magnetization reversal in circularly exchange-biased ferromagnetic disks. *Physical Review B* **2009**, *79*, 014436.
- [112] Masseboeuf, A.; Gatel, C.; Bayle-Guillemaud, P.; Lamy, Y.; Viala, B., The use of Lorentz microscopy for the determination of magnetic reversal mechanism of exchange-biased Co30Fe70/NiMn bilayer. *Journal of Magnetism and Magnetic Materials* **2009**, *321*, 3080-3083.
- [113] McCray, A. R. C.; Lebedev, D.; Arpaci, S.; te Velthuis, S. G. E.; Lopez-Dominguez, V.; Amiri, P. K.; Hersam, M. C.; Petford-Long, A. K.; Phatak, C., Control of Magnetic Skyrmions in an Exchange Biased van der Waals Ferromagnet. *Microscopy and Microanalysis* **2023**, *29*, 1710-1711.
- [114] Phatak, C.; Petford-Long, A. K.; De Graef, M., Recent advances in Lorentz microscopy. *Current Opinion in Solid State and Materials Science* **2016**, *20*, 107-114.
- [115] Kohno, Y.; Seki, T.; Findlay, S. D.; Ikuhara, Y.; Shibata, N., Real-space visualization of intrinsic magnetic fields of an antiferromagnet. *Nature* **2022**, *602*, 234-239.
- [116] Nguyen, K. X.; Huang, J.; Karigerasi, M. H.; Kang, K.; Cahill, D. G.; Zuo, J.-M.; Schleife, A.; Shoemaker, D. P.; Huang, P. Y., Angstrom-scale imaging of magnetization in antiferromagnetic Fe2As via 4D-STEM. *Ultramicroscopy* **2023**, *247*, 113696.
- [117] van Aken, P. A.; Lauterbach, S., Strong magnetic linear dichroism in Fe L23 and O K electron energy-loss near-edge spectra of antiferromagnetic hematite α -Fe2O3. *Physics and Chemistry of Minerals* **2003**, *30*, 469-477.
- [118] Qiu, Z. Q.; Bader, S. D., Surface magneto-optic Kerr effect. *Review of Scientific Instruments* **2000**, 71, 1243-1255.
- [119] Hubert, A.; Schäfer, R., Magnetic Domains: The Analysis of Magnetic Microstructures. Springer: Berlin, 2014.
- [120] Uchimura, T.; Yoon, J.-Y.; Sato, Y.; Takeuchi, Y.; Kanai, S.; Takechi, R.; Kishi, K.; Yamane, Y.; DuttaGupta, S.; Ieda, J. i.; Ohno, H.; Fukami, S., Observation of domain structure in non-collinear antiferromagnetic Mn3Sn thin films by magneto-optical Kerr effect. *Applied Physics Letters* **2022**, *120*.
- [121] Kang, K.; Yang, K.; Puthalath, K.; Cahill, D. G.; Schleife, A., Polar magneto-optical Kerr effect in antiferromagnetic \${M} {2}\mathrm{As}

- (M=\mathrm{Cr},\mathrm{Mn},\mathrm{Fe})\$ under an external magnetic field. *Physical Review B* **2022**, *105*, 184404.
- [122] Jourdan, M.; Bräuning, H.; Sapozhnik, A.; Elmers, H. J.; Zabel, H.; Kläui, M., Epitaxial Mn2Au thin films for antiferromagnetic spintronics. *Journal of Physics D: Applied Physics* **2015**, *48*, 385001.
- [123] Saidl, V.; Němec, P.; Wadley, P.; Hills, V.; Campion, R. P.; Novák, V.; Edmonds, K. W.; Maccherozzi, F.; Dhesi, S. S.; Gallagher, B. L.; Trojánek, F.; Kuneš, J.; Železný, J.; Malý, P.; Jungwirth, T., Optical determination of the Néel vector in a CuMnAs thin-film antiferromagnet. *Nature Photonics* **2017**, *11*, 91-96.
- [124] Zhou, C.; Xu, J.; Wu, T.; Wu, Y., Perspective on imaging antiferromagnetic domains in thin films with the magneto-optical birefringence effect. *APL Materials* **2023**, *11*.
- [125] Fiebig, M.; Pavlov, V. V.; Pisarev, R. V., Second-harmonic generation as a tool for studying electronic and magnetic structures of crystals: review. *J. Opt. Soc. Am. B* **2005**, *22*, 96-118.
- [126] Franken, P. A.; Hill, A. E.; Peters, C. W.; Weinreich, G., Generation of Optical Harmonics. *Physical Review Letters* **1961**, *7*, 118-119.
- [127] Fiebig, M.; Fröhlich, D.; Krichevtsov, B. B.; Pisarev, R. V., Second Harmonic Generation and Magnetic-Dipole-Electric-Dipole Interference in Antiferromagnetic \${\mathrm{Cr}} {2}\$\${\mathrm{O}} {3}\$. Physical Review Letters 1994, 73, 2127-2130.
- [128] Pisarev, R. V.; Sänger, I.; Petrakovskii, G. A.; Fiebig, M., Magnetic-Field Induced Second Harmonic Generation in ${\mathrm{C}}\operatorname{E}_{0}, {\mathrm{B}}_{2} {\mathrm{B}}. Physical Review Letters 2004, 93, 037204.$
- [129] Gao, C. L.; Wulfhekel, W.; Kirschner, J., Revealing the Antiferromagnetic Neel Structure in Real Space: One Monolayer Mn on Ag(111). *Physical Review Letters* **2008**, *101*, 267205.
- [130] Altfeder, I.; Yi, W.; Narayanamurti, V., Spin-polarized scanning tunneling microscopy of the room-temperature antiferromagnet \$c\$-FeSi. *Physical Review B* **2013**, *87*, 020403.
- [131] Sharma, S.; Li, H.; Ren, Z.; Castro, W. A.; Zeljkovic, I., Nanoscale visualization of the thermally driven evolution of antiferromagnetic domains in FeTe thin films. *Physical Review Materials* **2023**, *7*, 074401.
- [132] Ajayi, T. M.; Shirato, N.; Rojas, T.; Wieghold, S.; Cheng, X.; Latt, K. Z.; Trainer, D. J.; Dandu, N. K.; Li, Y.; Premarathna, S.; Sarkar, S.; Rosenmann, D.; Liu, Y.; Kyritsakas, N.; Wang, S.; Masson, E.; Rose, V.; Li, X.; Ngo, A. T.; Hla, S.-W., Characterization of just one atom using synchrotron X-rays. *Nature* **2023**, *618*, 69-73.
- [133] Sass, P. M.; Ge, W.; Yan, J.; Obeysekera, D.; Yang, J. J.; Wu, W., Magnetic Imaging of Domain Walls in the Antiferromagnetic Topological Insulator MnBi2Te4. *Nano Letters* **2020**, *20*, 2609-2614.
- [134] Kosub, T.; Kopte, M.; Hühne, R.; Appel, P.; Shields, B.; Maletinsky, P.; Hübner, R.; Liedke, M. O.; Fassbender, J.; Schmidt, O. G.; Makarov, D., Purely antiferromagnetic magnetoelectric random access memory. *Nature Communications* **2017**, *8*, 13985.
- [135] Finco, A.; Haykal, A.; Fusil, S.; Kumar, P.; Dufour, P.; Forget, A.; Colson, D.; Chauleau, J.-Y.; Viret, M.; Jaouen, N.; Garcia, V.; Jacques, V., Imaging Topological Defects in a Noncollinear Antiferromagnet. *Physical Review Letters* **2022**, *128*, 187201.
- [136] Healey, A. J.; Rahman, S.; Scholten, S. C.; Robertson, I. O.; Abrahams, G. J.; Dontschuk, N.; Liu, B.; Hollenberg, L. C. L.; Lu, Y.; Tetienne, J.-P., Varied Magnetic Phases in a van der Waals Easy-Plane Antiferromagnet Revealed by Nitrogen-Vacancy Center Microscopy. *ACS*

- Nano 2022, 16, 12580-12589.
- [137] Reichlova, H.; Janda, T.; Godinho, J.; Markou, A.; Kriegner, D.; Schlitz, R.; Zelezny, J.; Soban, Z.; Bejarano, M.; Schultheiss, H.; Nemec, P.; Jungwirth, T.; Felser, C.; Wunderlich, J.; Goennenwein, S. T. B., Imaging and writing magnetic domains in the non-collinear antiferromagnet Mn3Sn. *Nature Communications* **2019**, *10*, 5459.
- [138] Kaiser, U.; Schwarz, A.; Wiesendanger, R., Magnetic exchange force microscopy with atomic resolution. *Nature* **2007**, *446*, 522-525.
- [139] Amin, O. J.; Poole, S. F.; Reimers, S.; Barton, L. X.; Dal Din, A.; Maccherozzi, F.; Dhesi, S. S.; Novák, V.; Krizek, F.; Chauhan, J. S.; Campion, R. P.; Rushforth, A. W.; Jungwirth, T.; Tretiakov, O. A.; Edmonds, K. W.; Wadley, P., Antiferromagnetic half-skyrmions electrically generated and controlled at room temperature. *Nature Nanotechnology* **2023**, *18*, 849-853.
- [140] Liu, X.; Feng, Q.; Zhang, D.; Deng, Y.; Dong, S.; Zhang, E.; Li, W.; Lu, Q.; Chang, K.; Wang, K., Topological Spin Textures in a Non-Collinear Antiferromagnet System. *Advanced Materials* **2023**, *35*, 2211634.
- [141] Meer, H.; Gomonay, O.; Schmitt, C.; Ramos, R.; Schnitzspan, L.; Kronast, F.; Mawass, M.-A.; Valencia, S.; Saitoh, E.; Sinova, J.; Baldrati, L.; Kläui, M., Strain-induced shape anisotropy in antiferromagnetic structures. *Physical Review B* **2022**, *106*, 094430.
- [142] Gomonay, O.; Bossini, D., Linear and nonlinear spin dynamics in multi-domain magnetoelastic antiferromagnets. *Journal of Physics D: Applied Physics* **2021**, *54*, 374004.
- [143] Sánchez-Tejerina, L.; Puliafito, V.; Khalili Amiri, P.; Carpentieri, M.; Finocchio, G., Dynamics of domain-wall motion driven by spin-orbit torque in antiferromagnets. *Physical Review B* **2020**, *101*, 014433.
- [144] Khalili Amiri, P., Spin torques join forces in a memory device. *Nature Electronics* **2018**, *1*, 576-577.
- [145] Wang, K. L.; Amiri, P. K., Nonvolatile Spintronics: Perspectives on Instant-on Nonvolatile Nanoelectronic Systems. *SPIN* **2012**, *02*, 1250009.
- [146] Gomonay, E. V.; Loktev, V. M., Spintronics of antiferromagnetic systems (Review Article). *Low Temperature Physics* **2014**, *40*, 17-35.
- [147] Wolba, B.; Gomonay, O.; Kravchuk, V. P., Chaotic antiferromagnetic nano-oscillator driven by spin torque. *Physical Review B* **2021**, *104*, 024407.
- [148] Puliafito, V.; Sanchez-Tejerina, L.; Carpentieri, M.; Azzerboni, B.; Finocchio, G., Modulation, Injection Locking, and Pulling in an Antiferromagnetic Spin-Orbit Torque Oscillator. *IEEE Transactions on Magnetics* **2021**, *57*, 1-6.
- [149] Sizov, F.; Rogalski, A., THz detectors. Progress in Quantum Electronics 2010, 34, 278-347.
- [150] Safin, A.; Puliafito, V.; Carpentieri, M.; Finocchio, G.; Nikitov, S.; Stremoukhov, P.; Kirilyuk, A.; Tyberkevych, V.; Slavin, A., Electrically tunable detector of THz-frequency signals based on an antiferromagnet. *Applied Physics Letters* **2020**, *117*, 222411.